On the Computation of Equilibria of Elastic Rods Part I: Integrals, Symmetry and a Hamiltonian Formulation

Y. Li*
Texas Institute for Computational and Applied Mathematics
The University of Texas at Austin
Austin, TX 78713
yiwei@ticam.utexas.edu

J. H. Maddocks†
Institute for Physical Science and Technology
and Department of Mathematics
University of Maryland, College Park, MD 20742
jhm@ipst.umd.edu

May 22, 1996

Submitted to J. Computational Physics

*Partially supported by grants from the NSF and ONR.
†Partially supported by grants from the AFOSR and ONR.

Abstract

The equilibrium conditions for a hyper-elastic rod are formulated as a nonlinear, parameter dependent, two-point boundary value problem involving a Hamiltonian system of ordinary differential equations. A particularly efficient numerical formulation is achieved by exploiting Euler parameters combined with discretization via Gaussian collocation. The primary focus is on the particular problem of a closed twisted loop, which is a prototypical example for the study of super-coiling in DNA molecules. The highly symmetric case of a uniformly isotropic rod is shown to have intricately connected branches of solutions corresponding to changes in the imposed twist. Due to the presence of continuous symmetries, each equilibrium at fixed loading is non-isolated, and our numerical continuation techniques must account for this fact. It is also shown that the solution set for the symmetric case can be used as an organizing center for the computation of the disconnected set of equilibria of non–uniform, non–isotropic rods, via continuation and symmetry breaking techniques. The Hamiltonian structure of the governing equations is central to our numerical techniques for dealing with both the non–isolation of equilibria in the symmetric case, and the symmetry breaking required for the general case.

Key Words: elastica, rod, Hamiltonian, continuous symmetry, DNA, super-coiling, Euler parameters, continuation, symmetry breaking.

Math Subject Classification: 65P30, 65L10, 73C50, 92C40

1 Introduction

This article is the first in a three part series in which we develop a Hamiltonian model and associated numerical continuation code for the computation of the three-dimensional, large-deformation equilibrium configurations of elastic rods that are subject to twist and other two–point boundary loadings. The ultimate objective is a consistent hierarchy of computationally efficient models that encompass effects of non–uniformity, unequal bending stiffnesses, intrinsic curvature of the unstressed state, shear and extension and self–contact, all within a context that allows efficient numerical construction—through parameter continuation and branch switching techniques—of the rather complicated bifurcation sets that can arise. The primary focus of Part I is on the implications of the presence of continuous symmetries for the numerical computation of the solution set; in particular how the Hamiltonian structure and integrals of our model equations can be exploited to considerable advantage. In this work, we consider unshearable, inextensible rods, and ignore effects of self-contact. In Part II we extend the model to include self–contact forces that preclude self–intersections of the rod and allow the modelling of inter-wound equilibria, and in Part III we describe the modifications necessary to treat a shearable, extensible rod, and present more details of various bifurcation analyses.

The particular boundary value problem that is our primary concern is one in which a rod is twisted and then closed upon itself to form a stressed loop. Various versions of this example have now received considerable attention as an elementary prototype with which to develop a better understanding of the super-coiling of DNA (cf. e.g. [3], [4], [19], [23], [33], [34], [35], [37], [39], [40], references therein, and the extensive surveys [29] and [32]). Indeed potential applications to modelling DNA provided the primary motivation for this research, and in a companion work [28] the model developed here is exploited in a detailed study of the comparative cyclization rates of various short DNA segments. However there is little in our analysis or computational methods for dealing with continuous symmetries that is specific to the context of modelling DNA. In fact, while we only explicitly consider the particular equations arising from rod mechanics, the techniques we develop appear to be generally applicable to parameter-dependent, two-point boundary value problems for systems of ordinary differential equations with a Hamiltonian structure and invariance under a continuous symmetry group.

We develop a formulation of the equilibrium conditions for an unshearable, inextensible, elastic rod, or *elastica*, as a two–point boundary value problem for a Hamiltonian system of ordinary differential equations. We first consider the symmetric case of a uniformly isotropic rod in which the Hamiltonian system is completely integrable (in the classic sense pertaining to initial value problems). For the simplest boundary conditions describing a loop, the two continuous symmetries of uniformity and isotropy also yield families of explicit 'trivial' solutions, namely uniformly twisted solutions in which the centerline of the rod lies on a circle. Effects of self-contact are neglected throughout Part I, so we include in our discussion multiply-covered circular solutions in which the centerline of the rod traces the circumference of the circle an integer number of times. There are known families of bifurcation points on these families of twisted circular solutions, and we here show how to compute the branches of non–planar equilibria that emanate from those bifurcation points. The branches in the resulting solution set, or bifurcation diagram, have an intricate, but well-defined, pattern of connectivity (cf. Figure 5.2). Our computations also reveal that self-contact of the rod only arises in rather special well-defined circumstances (see Section 5). Away from these self-contact solutions, the centerlines of the equilibria have a well-defined torus knot type. Moreover equilibria for an arbitrary torus knot type can be found.

To be effective, numerical parameter continuation requires both that a starting point on each connected component of the solution set be known, and that each solution at a fixed parameter value be isolated. For the boundary value problem describing a closed loop of an elastica, it is the symmetries of uniformity and isotropy that give rise to the explicit families of circular solutions that yield known starting points for the continuation. The presence of these symmetries is also directly related to the connectedness of the solution set. However, at least for the most obvious boundary conditions describing the loop, the very same symmetries also imply that for any given load parameter, each equilibrium is non–isolated. The main mathematical point of interest in our analysis is the exploitation of the Hamiltonian structure and associated, symmetry–generated integrals to modify the boundary value problem in such a way that symmetries are factored out, and efficient numerical parameter continuation can be achieved. In particular for every boundary condition that is added, one should be discarded in order that the discretized problem will involve the numerical solution of square linear systems. The presence of integrals of the Hamiltonian, which can be regarded as convecting information from one boundary to the other, allows us to follow this prescription in a reasonably systematic fashion.

We also demonstrate that the connected solution set of the highly symmetric uniform, isotropic rod can be exploited as an organizing center for the computation of the branches of equilibria of general rods. In the absence of symmetry, no closed form solution is known that could serve as a direct starting point for numerical continuation of branches of equilibria. We avoid this difficulty by starting from solutions to the symmetric case, and show how to break the symmetries in a numerically robust manner. By starting from different points on the connected solution set of the symmetric problem, and breaking the symmetry, we are able to compute many disconnected components of the solution set of non–uniform, non–isotropic rods.

The structure of the article is as follows. In Section 2 we briefly review the coordinate free theory of the three–dimensional elastica. In Section 3 the Euler parameter description of proper rotations is introduced, and the associated Hamiltonian form of the elastica equilibrium equations is detailed. In Section 4, we verify our formulation and accuracy of the numerical code by computing explicitly known solutions of the comparatively-simple strut boundary value problem. We also use the strut example to introduce our techniques for both eliminating and breaking symmetries. In Section 5 the computations for a twisted uniform, isotropic loop are presented, and in Section 6 the results of symmetry breaking are described. Finally, a summary and discussion are presented in Section 7.

2 The Director Theory of Rods

In this section we summarize the theory of special Cosserat rods in exactly the form that will subsequently be used in our computations. Within the continuum mechanics literature, the model is considered to be a standard description of an inextensible, unshearable rod or *elastica* (cf. e.g. [1]).

2.1 Directors

The configuration of an elastica is described by the specification of two smooth vector functions

$$\mathbf{r}(s),\ \ \mathbf{d}_1(s): \quad [0,1] \to \mathbb{R}^3.$$

Here $\mathbf{r}(s)$ describes the *centerline* (or *line of centroids* or *axis*) of the rod, and $\mathbf{d}_1(s)$ is chosen to be a material unit vector lying in the normal cross–section at s. The rod is assumed to be inextensible so the variable s can, with suitable normalization, be interpreted as arc–length along the axis in any configuration. Given $\mathbf{d}_1(s)$, the orientation of the material cross–section at s in any configuration is also specified because, by the assumption of unshearability, material normal cross-sections remain undeformed and normal to the deformed axis.

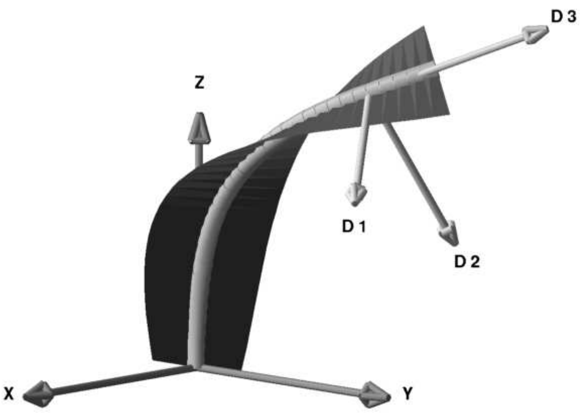

FIG. 2.1 *A representative ribbon describing the configuration of an elastica. The tube in the center of the ribbon represents the centerline of the rod and is parameterized by its arc-length s. The attached ribbon illustrates twisting of the rod. The orthonormal triad of directors $\mathbf{d}_1$, $\mathbf{d}_2$ and $\mathbf{d}_3$ can be regarded as indicating the orientation of a cross-section of the rod, with $\mathbf{d}_3$ tangent to the centerline, and $\mathbf{d}_1$ tangent to the ribbon.*

The condition of inextensibility implies that $\mathbf{r}'(s)$ is a unit vector, denoted $\mathbf{d}_3(s)$. (Here and throughout $'$ denotes a derivative with respect to arclength s.) A right–handed orthonormal basis $\{\mathbf{d}_1, \mathbf{d}_2, \mathbf{d}_3\}$, called the *directors*, may then be defined, in which $\mathbf{d}_2 = \mathbf{d}_3 \times \mathbf{d}_1$. The s-dependent orthonormal basis $\{\mathbf{d}_i(s)\}$ will later be related, *via* Euler parameters, to the fixed orthonormal basis $\{\mathbf{X}, \mathbf{Y}, \mathbf{Z}\}$. The configuration of the rod is fully determined if the functions $\mathbf{d}_i(s)$, $i = 1, 2, 3$, are specified, and *vice versa*. The function $\mathbf{r}(s)$ can always be recovered from the differential equation

$$\mathbf{r}'(s) = \mathbf{d}_3(s), \qquad \mathbf{r}(0) = \mathbf{r}_0. \tag{2.1}$$

As s varies the basis $\{\mathbf{d}_i(s)\}$ changes smoothly relative to the fixed basis and as the directors are orthonormal the change can be expressed as

$$\mathbf{d}_i' = \mathbf{u} \times \mathbf{d}_i, \qquad i = 1, 2, 3, \tag{2.2}$$

where the vector $\mathbf{u}$ is often called the *Darboux* vector. The components $u_i \equiv \mathbf{u} \cdot \mathbf{d}_i$ of the vector $\mathbf{u}$ with respect to the directors $\{\mathbf{d}_i\}$ are the components of strain associated with bending and twist. The triple of coordinates is denoted

$$\mathsf{u}(s) = (u_1(s),\, u_2(s),\, u_3(s)). \tag{2.3}$$

Knowledge of $u_1(s)$ and $u_2(s)$ is equivalent to knowledge of the curvature and geometrical torsion of the axis regarded as a space–curve. The strain $u_3(s)$ measures physical twist; it is not the geometrical torsion which is a property of the centerline only. The quantity $u_3(s)$, which will here always be referred to as *twist rate*, is the same as the quantity that is often referred to as *torsion* in the engineering literature.

2.2 Coordinate-Free Equilibrium Equations

It happens that convenient dependent variables for our analysis will be the Euler parameters alluded to earlier. However it is illuminating first to consider coordinate–free equilibrium equations, constitutive relations and boundary conditions.

The stresses acting across each material normal cross–section are equivalent to a force and a moment applied at the centroid of the cross–section at $\mathbf{r}(s)$; let $\mathbf{n}(s)$ and $\mathbf{m}(s)$ denote, respectively, this resultant force and moment (of the material on the side s^+ acting on the material on the side s^-). We will here assume that the only external loads are couples and forces applied at the ends of the rod. (For the self–contact problems that will be considered in Part II of this work, external distributed loads will be included.) The equilibrium equations are

$$\mathbf{n}'(s) = \mathbf{0}\,, \tag{2.4}$$

and

$$\mathbf{m}'(s) + \mathbf{r}'(s) \times \mathbf{n}(s) = \mathbf{0}. \tag{2.5}$$

Equation (2.4) has the integral

$$\mathbf{n}(s) = \mathbf{n}(0)\,, \tag{2.6}$$

so that equation (2.5) has the integral

$$\mathbf{m}\,(s)\; +\; \mathbf{r}\,(s) \times \mathbf{n}\,(s) = \boldsymbol{\xi}\,. \tag{2.7}$$

Here $\boldsymbol{\xi}$ is a constant vector which, by choice of origin for $\mathbf{r}$, can be chosen to be parallel to $\mathbf{n}$. From (2.6) and (2.7) we have that

$$\mathbf{m}(s) \cdot \mathbf{n}(s) = \mathbf{m}(0) \cdot \mathbf{n}(0) . \tag{2.8}$$

When evaluated at $s = 1$, equations (2.6) and (2.8) provide relations between the boundary conditions at $s = 0$ and those at $s = 1$ that are implied by the balance of external forces and moments acting on the elastica. Such relations will be central in the development of our techniques for modifying boundary conditions to eliminate symmetry–induced non–isolation of equilibria in a manner allowing efficient numerical continuation methods to be applied.

2.3 Constitutive Relations

In order to proceed further it is necessary to introduce constitutive relations between the strains and the resultant forces and moments appearing in our rod model. In point of fact, because we assume the rod to be inextensible and unshearable, the components of the resultant force $\mathbf{n}$ are basic unknowns. In contrast, the components of the bending and twist moment $\mathbf{m}$ are related to the bending and twist strains u_i, introduced in (2.3). In order to specify this constitutive relation some further notation is required. The triple of components $m_i(s) \equiv \mathbf{m}(s) \cdot \mathbf{d}_i(s)$ will be denoted $\mathsf{m} = (m_1, m_2, m_3)$. We also allow the unstressed configuration of the rod to have intrinsic curvature and twist. The strains at this unstressed state will be denoted $\hat{\mathsf{u}}(s) = (\hat{u}_1(s), \hat{u}_2(s), \hat{u}_3(s)\,)$ with the $\hat{u}_i(s)$ being prescribed functions. The unstressed configuration is straight when $\hat{u}_1(s) \equiv \hat{u}_2(s) \equiv 0$. If in addition $\hat{u}_3(s) \equiv 0$, the unstressed state is prismatic or untwisted.

We shall only consider the case in which the rod is hyper-elastic, i.e. there exists a scalar–valued strain energy density function $W(\mathsf{u} - \hat{\mathsf{u}}, s)$, dependent upon the three strain measures $u_i - \hat{u}_i$, and arc–length s, with the property that

$$m_i = \frac{\partial W}{\partial u_i}, \qquad i = 1,\, 2,\, 3 . \tag{2.9}$$

Following common practice, we shall assume that the function W is a strictly convex function of the three arguments $(u_i - \hat{u}_i)$, with a minimum at $W(0,\, 0,\, 0,\, s)$.

For computation, a specific form of W must be chosen and we will focus here upon the case where the rod is assumed to be linearly elastic, that is, the strain energy density function is quadratic in the u_i. Explicitly

$$W(\mathsf{u} - \hat{\mathsf{u}},\, s) = \frac{1}{2} K_1 (u_1 - \hat{u}_1)^2 + \frac{1}{2} K_2 (u_2 - \hat{u}_2)^2 + \frac{1}{2} K_3 (u_3 - \hat{u}_3)^2, \tag{2.10}$$

with

$$m_i = \frac{\partial W}{\partial u_i} = K_i(u_i - \hat{u}_i)\,, \qquad i = 1,\,2,\,3\,. \tag{2.11}$$

Here the bending and twist stiffnesses $K_i(s)$ are prescribed positive functions of s, possibly constant.

Models of rod mechanics often begin with the assumption that the rod is a solid object whose diameter is small compared to its length. This is the approach taken in the theory of Kirchhoff and Clebsch, as described in [25], for example. If we adopt this point of view, and also assume that the material composing the rod is homogeneous and isotropic, then we can further interpret the elastic coefficients as $K_1 = EI_1$, $K_2 = EI_2$ and $K_3 = GI_3$, where I_i is the geometric moment of the planar cross–section about the $\mathbf{d}_i$ axis (so that $I_3 = I_1 + I_2$), E is the Young's modulus, $G = E/[2(1+\nu)]$ is the shear modulus, and ν is Poisson's ratio. However, in other applications, such as modelling a DNA molecule with a continuum rod approximation, the elastic coefficients K_i may not have such an interpretation, and instead should be viewed as the coefficients in the first terms of a Taylor expansion of a more complicated constitutive relation. In any case, one could consider strain energies more general than that given by equation (2.10). Our analysis depends only on the general hyper-elastic form (2.9), and the associated computations could be carried out for any specific choice of strain energy density function. With some minor modifications one could even consider a strain energy that is not a convex function of the strains (cf. [18]).

2.4 Boundary Conditions

There are many possible boundary conditions that can be physically appropriate for rods. Here we consider only three that can readily be approximated in experiment. First, it can be specified that the moment $\mathbf{m}$ vanish at a free end; for example, one can specify the boundary conditions

$$\mathbf{m}(1) = \mathbf{0}.$$

Second, it is possible to specify completely the orientation of one end of the rod with respect to the fixed basis $\{\mathbf{i}, \mathbf{j}, \mathbf{k}\}$. This condition is equivalent to specifying two, and consequently all three, of the directors $\{\mathbf{d}_i\}$. For example,

$$\mathbf{d}_1(0) = \mathbf{i}\,, \quad \mathbf{d}_2(0) = \mathbf{j}\,, \quad \mathbf{d}_3(0) = \mathbf{k}\,.$$

These last boundary conditions taken together with a specified value of $\mathbf{r}(0)$ describe a *clamped end*. Third, it is possible to specify only the direction of the tangent to the axis at one end; for example,

$$\mathbf{d}_3(1) = \mathbf{i}\,.$$

3 The Governing Equations

In this section we develop the Hamiltonian system of ordinary differential equations that will provide the basis for our computations. We first describe the Euler parameter description of the directors $\mathbf{d}_i$. We then introduce a variational form of the equilibrium conditions, and the associated Lagrangian and Hamiltonian forms of the governing equations. Finally we describe the symmetries and associated integrals of the governing Hamiltonian system.

3.1 Representation of Directors by Euler Parameters

Thus far we have not specified any particular parameterization of the directors $\{\mathbf{d}_i(s)\}$. For three-dimensional equilibria, a parameterization of the directors $\{\mathbf{d}_i(s)\}$ is equivalent to selecting a representation for the group of proper orthogonal transformations $SO(3)$. In mechanics there are several common choices for such a representation (cf. e.g. [16]). Euler angles are often adopted because they involve the minimum number of variables, namely three, but there are two significant drawbacks in their use. First, due to the topology of $SO(3)$, a set of three parameters cannot provide a nonsingular, global representation. In the case of Euler angles there is a direction in space at which the representation becomes singular, and significant computational awkwardness can arise if inaccuracies are to be avoided close to the singularity. A second drawback in the use of Euler angles is the ubiquitous appearance of trigonometric functions.

Euler parameters are an alternative choice that provide a global (i.e. singularity free), four parameter, two–to–one description of $SO(3)$. In addition, only rational polynomial functions arise in the representation. A difficulty with Euler parameters is that they are not independent—the squares of the four parameters must sum to one—which imposes a constraint that can lead to awkwardness in numerical discretization. However this constraint fits very naturally into our numerical treatment of the Hamiltonian version of the governing equations. An elementary discussion of Euler parameters can be found, for example, in [16], but we here present a self–contained summary of the kinematics that will be required.

A set of Euler parameters is a quadruple of real numbers

$$\mathbf{q} = (q_1, q_2, q_3, q_4)$$

that satisfy the identity

$$\mathbf{q} \cdot \mathbf{q} = {q_1}^2 + {q_2}^2 + {q_3}^2 + q_4^2 = 1 \ . \tag{3.12}$$

In other words a set of Euler parameters, or *unit quaternion*, is an element of the unit sphere $\mathbf{S}^3$ in $\mathbb{R}^4$.

From Euler's theorem on rotations, the relative orientation of two reference frames can be expressed as a simple rotation about a fixed axis. Let $\mathbf{a} = a_1\mathbf{i} + a_2\mathbf{j} + a_3\mathbf{k}$ denote the unit vector parallel to this axis, and θ be the angle of rotation. Then the associated Euler parameters are

$$q_4 = \cos(\theta/2)\,, \tag{3.13}$$

and

$$q_i = a_i \sin(\theta/2), \qquad i = 1,\, 2,\, 3. \tag{3.14}$$

Obviously if $\mathbf{q}$ corresponds to a simple rotation $(\mathbf{a}, \theta)$, then $-\mathbf{q}$ corresponds to the equivalent simple rotation $(\mathbf{a}, \theta + 2\pi)$. Therefore there is a two–to–one correspondence between Euler parameters and simple rotations.

The components of the orthonormal triad $\{\mathbf{d}_i\}$ (with respect to the fixed space basis) in terms of a set of Euler parameters $\mathbf{q}$ are given by:

$$\mathbf{d}_1 = \begin{pmatrix} q_1^2 - q_2^2 - q_3^2 + q_4^2 \\ 2(q_1q_2 + q_3q_4) \\ 2(q_1q_3 - q_2q_4) \end{pmatrix}, \quad \mathbf{d}_2 = \begin{pmatrix} 2(q_1q_2 - q_3q_4) \\ -q_1^2 + q_2^2 - q_3^2 + q_4^2 \\ 2(q_2q_3 + q_1q_4) \end{pmatrix}, \tag{3.15}$$

$$\mathbf{d}_3 = \begin{pmatrix} 2(q_1q_3 + q_2q_4) \\ 2(q_2q_3 - q_1q_4) \\ -q_1^2 - q_2^2 + q_3^2 + q_4^2) \end{pmatrix}. \tag{3.16}$$

The strains u_i appearing in equations (2.2) are given in terms of the Euler parameters by (see, for example, Dichmann [6] or Kane [20])

$$u_i = \frac{2\mathbf{q}' \cdot \mathbf{B}_i\mathbf{q}}{|\mathbf{q}|^2}\,, \qquad i = 1,\, 2,\, 3. \tag{3.17}$$

Here the $\mathbf{B}_i$ are 4×4 skew–symmetric matrices:

$$\mathbf{B}_1 = \begin{pmatrix} 0 & 0 & 0 & 1 \\ 0 & 0 & 1 & 0 \\ 0 & -1 & 0 & 0 \\ -1 & 0 & 0 & 0 \end{pmatrix}, \quad \mathbf{B}_2 = \begin{pmatrix} 0 & 0 & -1 & 0 \\ 0 & 0 & 0 & 1 \\ 1 & 0 & 0 & 0 \\ 0 & -1 & 0 & 0 \end{pmatrix},$$

$$\mathbf{B}_3 = \begin{pmatrix} 0 & 1 & 0 & 0 \\ -1 & 0 & 0 & 0 \\ 0 & 0 & 0 & 1 \\ 0 & 0 & -1 & 0 \end{pmatrix}.$$

For any set of Euler parameters the vectors $\{\mathbf{B}_i\mathbf{q}\}$, together with $\mathbf{q}$, form an orthonormal basis for $\mathbb{R}^4$. Geometrically, the vector $\mathbf{B}_i\mathbf{q}$ acts as the infinitesimal generator of rotation about the ith director $\mathbf{d}_i$.

3.2 Variational Formulations

Using equation (3.17) to eliminate the strains, the strain energy density function can be written in terms of the Euler parameters and their derivatives

$$W(\mathsf{u} - \hat{\mathsf{u}},\, s) = W\left(\frac{2\mathbf{q}' \cdot \mathbf{B}_i\mathbf{q}}{|\mathbf{q}|^2} - \hat{u}_i,\, s\right). \tag{3.18}$$

In the case at hand, in which it is assumed that there are no distributed loads acting on the rod, the equilibrium configurations can then be characterized as constrained critical points of the energy functional

$$\int_0^1 W\left(\frac{2\mathbf{q}' \cdot \mathbf{B}_i\mathbf{q}}{|\mathbf{q}|^2} - \hat{u}_i,\, s\right) ds, \tag{3.19}$$

subject to the constraints,

$$\mathbf{r}'(s) = \mathbf{d}_3(\mathbf{q}(s)) \qquad \text{and} \qquad \mathbf{q}(s) \cdot \mathbf{q}'(s) = 0, \tag{3.20}$$

and appropriate boundary conditions, including the requirement that the Euler parameters have unit norm at one end point. Here $\mathbf{d}_3(\mathbf{q}(s))$ denotes the vector of quadratic functions of q_i defined in (3.16). By introducing Lagrange multiplier functions $\boldsymbol{\lambda}(s) \in \mathbb{R}^3$ and $\nu(s) \in \mathbb{R}$ associated with the pointwise constraints (3.20), the equilibrium configurations can be characterized as unconstrained critical points of the Lagrangian

$$\mathcal{L}(\mathbf{q}, \mathbf{q}', \mathbf{r}', \boldsymbol{\lambda}, \nu, s) = W\left(\frac{2\mathbf{q}' \cdot \mathbf{B}_i\mathbf{q}}{|\mathbf{q}|^2} - \hat{u}_i,\, s\right) + \boldsymbol{\lambda} \cdot (\mathbf{r}' - \mathbf{d}_3) + \nu\, \mathbf{q} \cdot \mathbf{q}'. \tag{3.21}$$

To justify the variational principle we need to demonstrate that the associated first–order conditions, or Euler–Lagrange equations, taken in conjunction with the constraints (3.20), are equivalent to the coordinate free, equilibrium conditions obtained earlier. The Euler–Lagrange equation of (3.21) with respect to the variable $\mathbf{r}$, namely

$$-\frac{d}{ds}\left[\frac{\partial \mathcal{L}}{\partial \mathbf{r}'}\right]+\frac{\partial \mathcal{L}}{\partial \mathbf{r}}=0,$$

reduces to

$$\boldsymbol{\lambda}'(s)=0,$$

which can be recognized as equation (2.4) for the resultant force $\mathbf{n}(s)$ acting across the cross–section of the rod. That is, the physical interpretation of the Lagrange multiplier $\boldsymbol{\lambda}(s)$ is as the constant force $\mathbf{n}$. Moreover, the first constraint appearing in (3.20) is exactly the equation appearing in (2.1).

It remains to consider the Euler–Lagrange equation with respect to the variable $\mathbf{q}$, namely

$$-\frac{d}{ds}\left[\frac{\partial \mathcal{L}}{\partial \mathbf{q}'}\right]+\frac{\partial \mathcal{L}}{\partial \mathbf{q}}=0, \tag{3.22}$$

which is a vector equation of dimension four. A short calculation of the explicit form of (3.22) leads to the following conclusions. First, the component in the direction $\mathbf{q}(s)$ implies that the multiplier $\nu(s)$ satisfies the equation

$$\nu'=-2\mathbf{n}\cdot\mathbf{d}_3\,, \tag{3.23}$$

or

$$\nu=-2\mathbf{n}\cdot\mathbf{r}+c\,. \tag{3.24}$$

Because ν multiplies a perfect derivative in the Lagrangian (3.21), it is apparent that the value taken for the integration constant c is immaterial to the governing equations. Second, the remaining three components of (3.22) in the directions $\mathbf{B}_1\mathbf{q}$, $\mathbf{B}_2\mathbf{q}$ and $\mathbf{B}_3\mathbf{q}$, reduce to the three components of the moment balance equation (2.5) with respect to the director frame $\{\mathbf{d}_i(s)\}$. The calculations exploit the skew-symmetry of the matrices $\mathbf{B}_i$, orthogonality of the $\mathbf{B}_i\mathbf{q}$, the constitutive relations (2.9), and the constraint $\mathbf{q}\cdot\mathbf{q}'=0$. (When writing (2.5) in components with respect to the non–constant director frame, it should also be recalled that $\mathbf{d}_i\cdot\mathbf{m}'=m_i'+\mathbf{d}_i\cdot(\mathbf{u}\times\mathbf{m})$. Alternatively equation (2.5) can be recovered directly by taking components of (3.22) with respect to the basis $\mathbf{F}_i\mathbf{q}$ introduced in Section 3.3, but the details are unimportant for our purposes.)

For our numerical treatment it is convenient to write the governing equations in the form of a first order system, and for the sake of analysis it is convenient to take the first-order system to be Hamiltonian. However the derivation of the appropriate Hamiltonian system is nonstandard for two reasons. First, because we have chosen to parameterize the three dimensional group $SO(3)$ using the four Euler parameters, the Lagrangian (3.21) is not a strictly convex function of the derivatives of the Euler parameters $\mathbf{q}'$. That issue is addressed by Dirac's theory of constraints (cf. e.g. [9]). Second, and not independently, in the Lagrangian (3.21) we have chosen to enforce the norm condition $|\mathbf{q}|^2 = 1$ by the introduction of a multiplier ν associated with the differentiated constraint $\mathbf{q} \cdot \mathbf{q}' = 0$. Consequently, the multiplier ν appears in the definition of the conjugate variable

$$\boldsymbol{\mu} \equiv \frac{\partial \mathcal{L}}{\partial \mathbf{q}'} = \frac{2}{|\mathbf{q}|^2} \sum_i W_{u_i} \mathbf{B}_i \mathbf{q} + \nu \mathbf{q}. \tag{3.25}$$

It is not necessary to pursue the full ramifications of this choice here; it is a simple example of the impetus–striction formulation of constrained dynamics as developed by Dichmann and co-authors [6], [8], combined with the Dirac theory to account for the absence of strict convexity. We shall refer to the conjugate variable $\boldsymbol{\mu}$ as the *impetus* with no further comment, and simply verify that a certain Hamiltonian yields the correct governing equations without a general discussion of how the Hamiltonian can be constructed.

The Hamiltonian system involves the (standard) Legendre transform $W^*(\mathsf{v}, s)$ of the constitutive function $W(\mathsf{w}, s)$ introduced in (2.9). We assume that

$$\frac{\partial W}{\partial \mathsf{w}}(0) = 0, \tag{3.26}$$

and that W is a strictly convex function of w, i.e.,

$$\frac{\partial^2 W}{\partial \mathsf{w}^2}(\mathsf{w}) > 0, \tag{3.27}$$

where for the moment we suppress the explicit s–dependence of W which merely acts as a parameter. Then the variables v conjugate to w are defined by

$$\mathsf{v} = \frac{\partial W}{\partial \mathsf{w}}(\mathsf{w})\,. \tag{3.28}$$

By the strict convexity assumption we can invert to solve for w, to get

$$\mathsf{w} = \phi(\mathsf{v})\,. \tag{3.29}$$

The Legendre transform is then defined to be

$$W^*(\mathsf{v}) = \mathsf{v} \cdot \phi(\mathsf{v}) - W(\phi(\mathsf{v})). \tag{3.30}$$

In the special case of a pure quadratic W,

$$W(\mathsf{w}) = \frac{1}{2} \sum_i K_i \, w_i^2 \,, \tag{3.31}$$

the conjugate variables are $v_i = K_i \, w_i$, and the Legendre transform is

$$W^*(\mathsf{v}) = \frac{1}{2} \sum_i \frac{v_i^2}{K_i}. \tag{3.32}$$

In our rod model, the general constitutive relation involves a function of the shifted variable $\mathsf{u} - \hat{\mathsf{u}}$. The variables conjugate to u are then the components of bending and twisting moment m defined in (2.9). Moreover, as can easily be verified, the Legendre transform of a function of a shifted variable, is the shift of the transform, so the Legendre transform of $W(\mathsf{u} - \hat{\mathsf{u}})$ with respect to the variable u is

$$W^*(\mathsf{m}) + \mathsf{m} \cdot \hat{\mathsf{u}}. \tag{3.33}$$

In the particular case of a quadratic strain energy density function, we obtain the Legendre transform

$$\sum_i \left(\frac{m_i^2}{2K_i(s)} + m_i \, \hat{u}_i \right) \,. \tag{3.34}$$

We claim that the Hamiltonian leading to the equations governing the equilibria of an elastica can now be written in the form

$$H(\mathbf{r}, \mathbf{q}, \mathbf{n}, \boldsymbol{\mu}, s) = W^*(\mathsf{m}, s) + \mathsf{m} \cdot \hat{\mathsf{u}}(s) + \mathbf{n} \cdot \mathbf{d}_3. \tag{3.35}$$

The phase space variables in this Hamiltonian formulation are the axis $\mathbf{r}$, the force $\mathbf{n}$ which is conjugate to $\mathbf{r}$, the Euler parameters $\mathbf{q}$, and their conjugate variable, namely the impetus $\boldsymbol{\mu}$. The right hand side of (3.35) can be written in terms of the phase variables by substituting the expression (3.16) for $\mathbf{d}_3(\mathbf{q})$ and by using the relations

$$m_i = \frac{1}{2} \boldsymbol{\mu} \cdot \mathbf{B}_i \mathbf{q} \, (= W_{u_i}(\mathsf{u} - \hat{\mathsf{u}})) \qquad i = 1, 2, 3, \tag{3.36}$$

which follow from the hyper-elastic constitutive relation (2.9) and the components of the definition (3.25) of $\boldsymbol{\mu}$ in the directions $\mathbf{B}_i \mathbf{q}$. The second equation in (3.36) can itself be further inverted using the implicitly defined inverse function ϕ introduced in equations (3.28) and (3.29), leading to the expression

$$\mathsf{u} = \hat{\mathsf{u}} + \phi\left(\frac{\boldsymbol{\mu}\cdot\mathbf{B}_1\mathbf{q}}{2}, \frac{\boldsymbol{\mu}\cdot\mathbf{B}_2\mathbf{q}}{2}, \frac{\boldsymbol{\mu}\cdot\mathbf{B}_3\mathbf{q}}{2}\right) \tag{3.37}$$

for the strains. In the particular case of linear elasticity, (3.37) simplifies to

$$u_i = \hat{u}_i + \frac{\boldsymbol{\mu}\cdot\mathbf{B}_i\mathbf{q}}{2\,K_i}, \qquad i = 1,\,2,\,3, \tag{3.38}$$

and the Hamiltonian takes the explicit form

$$H(\mathbf{r},\mathbf{q},\mathbf{n},\boldsymbol{\mu}) = \sum_{i=1}^{3}\left(\frac{m_i^2}{2\,K_i} + \hat{u}_i m_i\right) + \mathbf{n}\cdot\mathbf{d}_3. \tag{3.39}$$

The Hamiltonian system of equations governing equilibria is of the form

$$\left\{\begin{aligned}
\mathbf{r}' &= \frac{\partial H}{\partial \mathbf{n}} = \mathbf{d}_3,\\
\mathbf{q}' &= \frac{\partial H}{\partial \boldsymbol{\mu}} = \frac{1}{2}\sum_{i=1}^{3} u_i\,\mathbf{B}_i\mathbf{q},\\
\mathbf{n}' &= -\frac{\partial H}{\partial \mathbf{r}} = 0,\\
\boldsymbol{\mu}' &= -\frac{\partial H}{\partial \mathbf{q}} = \frac{1}{2}\sum_{i=1}^{3} u_i\,\mathbf{B}_i\boldsymbol{\mu} - \frac{\partial \mathbf{d}_3}{\partial \mathbf{q}}^T\mathbf{n},
\end{aligned}\right. \tag{3.40}$$

where again $\mathbf{d}_3(\mathbf{q})$ is defined by the formula (3.16), so that

$$\frac{\partial \mathbf{d}_3}{\partial \mathbf{q}} = 2\begin{pmatrix} q_3 & q_4 & q_1 & q_2\\ -q_4 & q_3 & q_2 & -q_1\\ -q_1 & -q_2 & q_3 & q_4 \end{pmatrix},$$

and the u_i are written in terms of the phase variables $\mathbf{q}$ and $\boldsymbol{\mu}$ using relation (3.37), or in the case of linear elasticity the explicit form (3.38). The fact that the expressions for the partial derivatives $\frac{\partial H}{\partial \boldsymbol{\mu}}$ and $\frac{\partial H}{\partial \mathbf{q}}$ involve the strains u_i in a simple way can be verified directly, but is a consequence of the chain rule and the property

$$\frac{\partial W^*(\mathsf{v})}{\partial \mathsf{v}} = \phi(\mathsf{v})$$

of the Legendre transform (3.30).

It is straightforward to verify that equations (3.40) form an appropriate set of governing equations. The first three equations are the unshearability and inextensibility constraint. The second set of four are the expression for $\mathbf{q}'$ that arises from the inversion of the kinematic relation (3.17). The necessary inversion uses the constraint $\mathbf{q}\cdot\mathbf{q}' = 0$ and the orthogonality of the basis $\{\mathbf{B}_i\mathbf{q}, \mathbf{q}\}$. The third set of three equations reflect the invariance of shear force with arc–length s. Finally, by construction, the fourth set of equations are equivalent to the explicit form of the Euler–Lagrange equations (3.22) of $\mathcal{L}$ with respect to the Euler–parameters $\mathbf{q}$, which were earlier argued to be equivalent to the balance of moments (2.5).

3.3 Analysis of Integrals and Symmetries

We next detail the integrals or conserved quantities of the Hamiltonian system (3.40), i.e., functions of the phase variables that are independent of arc–length s. We will later see the usefulness of these integrals in the choice of boundary conditions.

Six integrals are obtained immediately from equations (2.6) and (2.7). The three components of force $\mathbf{n}$ are constant due to the translational symmetry of the Hamiltonian system in space. Similarly the three components of $\mathbf{m} + \mathbf{r} \times \mathbf{n}$ are invariant as a consequence of rotational symmetry about the three inertial axes. To see that these expressions provide integrals of (3.40), we merely need to write them as functions of the phase variables. Components of $\mathbf{n}$ and $\mathbf{r}$ with respect to the fixed basis are trivially phase variables, and it can be verified that the components $\overline{m}_i$ of $\mathbf{m}$ with respect to the fixed space basis can be written as (cf. [6])

$$\overline{m}_i = \frac{1}{2}\boldsymbol{\mu} \cdot \mathbf{F}_i\mathbf{q}, \qquad i = 1,\, 2,\, 3, \tag{3.41}$$

where

$$\mathbf{F}_1 = \begin{pmatrix} 0 & 0 & 0 & 1 \\ 0 & 0 & -1 & 0 \\ 0 & 1 & 0 & 0 \\ -1 & 0 & 0 & 0 \end{pmatrix}, \quad \mathbf{F}_2 = \begin{pmatrix} 0 & 0 & 1 & 0 \\ 0 & 0 & 0 & 1 \\ -1 & 0 & 0 & 0 \\ 0 & -1 & 0 & 0 \end{pmatrix},$$

$$\mathbf{F}_3 = \begin{pmatrix} 0 & -1 & 0 & 0 \\ 1 & 0 & 0 & 0 \\ 0 & 0 & 0 & 1 \\ 0 & 0 & -1 & 0 \end{pmatrix}.$$

In addition to the integrals listed above which have physical interpretations, there are two integrals which arise from the representation of $SO(3)$ by the four Euler parameters, rather than by a three parameter description. By construction, the second equation of (3.40) implies

$$\mathbf{q} \cdot \mathbf{q}' = \frac{1}{2} \sum_{i=1}^{3} u_i \, \mathbf{q} \cdot \mathbf{B}_i \mathbf{q} = 0,$$

so that $|\mathbf{q}|^2$ is a seventh integral. The symmetry associated with the integral $|\mathbf{q}|^2$ is of some interest. The integral is generated by the symmetry $\boldsymbol{\mu} \longrightarrow \boldsymbol{\mu} + \epsilon \mathbf{q}$, which is a gauge freedom in the impetus variable associated with the non-convexity of the Lagrangian (3.21) with respect to the $\mathbf{q}'$ variable.

Next consider the quantity $\boldsymbol{\mu} \cdot \mathbf{q} + 2\mathbf{r} \cdot \mathbf{n}$. By virtue of (3.40), we find

$$\begin{aligned} \frac{d}{ds}(\boldsymbol{\mu} \cdot \mathbf{q} + 2\mathbf{r} \cdot \mathbf{n}) = \quad & -\mathbf{n} \cdot \frac{\partial \mathbf{d}_3}{\partial \mathbf{q}} \mathbf{q} + \frac{1}{2} \sum_{i=1}^{3} u_i \mathbf{q} \cdot \mathbf{B}_i \boldsymbol{\mu} \\ & + \frac{1}{2} \sum_{i=1}^{3} u_i \boldsymbol{\mu} \cdot \mathbf{B}_i \mathbf{q} + 2\mathbf{d}_3 \cdot \mathbf{n}. \end{aligned} \tag{3.42}$$

Euler's Theorem for homogeneous functions implies that $2\mathbf{d}_3 = \dfrac{\partial \mathbf{d}_3}{\partial \mathbf{q}} \mathbf{q}$. Moreover the matrices $\mathbf{B}_i$ are skew symmetric, so it follows that (3.42) vanishes and

$$\boldsymbol{\mu} \cdot \mathbf{q} + 2\mathbf{r} \cdot \mathbf{n} \tag{3.43}$$

is an eighth integral of the system. The integral (3.43) is associated with invariance of the Hamiltonian under the (variational) symmetry in which $\mathbf{q}$ is replaced by $(1+\epsilon)\mathbf{q}$, $\boldsymbol{\mu}$ is replaced by $(1+\epsilon)^{-1}\boldsymbol{\mu}$, $\mathbf{r}$ is replaced by $(1+\epsilon)^2\mathbf{r}$ and $\mathbf{n}$ is replaced by $(1+\epsilon)^{-2}\mathbf{n}$.

Notice that the multiplier ν appearing in the Lagrangian (3.21) is involved in the definition (3.25) of the impetus, but not explicitly in the Hamiltonian (3.39). From (3.25) and the unit norm condition on the Euler–parameters, we also see that

$$\boldsymbol{\mu} \cdot \mathbf{q} \equiv \nu.$$

The integral (3.43) can then be recognized as being equivalent to the expression (3.24) for the multiplier $\nu(s)$. In the Lagrangian form of the governing equation the value of the integration constant c in (3.24) is irrelevant. Similarly in the Hamiltonian form, specification of the value of the integral (3.43) merely eliminates the gauge freedom in $\boldsymbol{\mu}$.

The above integrals arise for all constitutive laws. There are two additional, constitutive dependent, integrals that arise in each of the cases of an *isotropic* rod, and a *uniform* rod. The tangential component of bending moment is

$$m_3(s) \equiv \mathbf{m} \cdot \mathbf{d}_3 = \frac{\boldsymbol{\mu} \cdot \mathbf{B}_3 \mathbf{q}}{2}$$

A straightforward computation, using (3.38), (3.40) and properties of the $\mathbf{B}_i$ matrices, reveals that

$$\begin{aligned} 2\frac{d}{ds} m_3(s) &= (\boldsymbol{\mu} \cdot \mathbf{B}_3 \mathbf{q}' + \boldsymbol{\mu}' \cdot \mathbf{B}_3 \mathbf{q}) = -u_1 \boldsymbol{\mu} \cdot \mathbf{B}_2 \mathbf{q} + u_2 \boldsymbol{\mu} \cdot \mathbf{B}_1 \mathbf{q} \\ &= (\boldsymbol{\mu} \cdot \mathbf{B}_1 \mathbf{q})\,(\boldsymbol{\mu} \cdot \mathbf{B}_2 \mathbf{q}) \left(\frac{1}{K_2} - \frac{1}{K_1} \right) - \hat{u}_1 \boldsymbol{\mu} \cdot \mathbf{B}_2 \mathbf{q} + \hat{u}_2 \boldsymbol{\mu} \cdot \mathbf{B}_1 \mathbf{q}\,. \end{aligned}$$

Accordingly, if $K_1(s) \equiv K_2(s)$ and $\hat{u}_1 \equiv \hat{u}_2 \equiv 0$, then $m_3(s) = \boldsymbol{\mu} \cdot \mathbf{B}_3 \mathbf{q}/2$ provides a ninth integral. This case will be described as a *transversely isotropic* or just *isotropic* rod. We have here only explicitly derived the condition of isotropy for a linearly elastic rod, but it extends to more general constitutive relations (see, e.g. [1] or [27]). The symmetry associated with the twist integral is a rotation of the rod about its own centerline.

A short calculation verifies that in isotropic rods the determination of the centerline $\mathbf{r}(\mathbf{s})$ and force $\mathbf{n}$ is largely decoupled from the twist rate $u_3(s)$; rather the crucial quantity is the (constant) value of the twist integral m_3. Consequently, if an equilibrium of a given isotropic rod is known, equilibria of other isotropic rods with the same centerline $\mathbf{r}(\mathbf{s})$ and force $\mathbf{n}$, but different coefficients $K_3(s)$ and $\hat{u}_3(s)$ can immediately be determined. The solutions differ only in the rate at which the directors spin about the tangent, with the rate being determined from equation (3.38) in the case $i = 3$

$$u_3 = \frac{m_3}{K_3} + \hat{u}_3, \tag{3.44}$$

where now m_3 is prescribed. This observation plays a pivotal role in the computations of DNA configurations that are presented in [28]. As is more fully explained there, the decoupling between twist and bending is associated with the freedom generated by the symmetry of isotropy to redefine the material director basis by rotating about the tangent vector $\mathbf{d}_3(s)$.

The second constitutive dependent symmetry is uniformity. If the constitutive function W has no explicit s dependence, which in the linearly elastic case means the stiffnesses K_i and the unstressed strains $\hat{u}_i$ are all constant, then the Hamiltonian $\mathcal{H}$ (3.35) has no explicit s dependence, and therefore represents a tenth integral of the system. The associated symmetry is translation in the arc-length s, or relabelling of the material point corresponding to $s = 0$.

An important but fine point, which is most easily described in the linearly elastic case, arises when the two bending stiffnesses $K_1 = K_2$ are equal and constant, and the unstressed state is straight, so that $\hat{u}_1 = \hat{u}_2 = 0$. Such rods are isotropic, but if the twist stiffness $K_3(s)$ and intrinsic twist rate $\hat{u}_3(s)$ are non-constant functions of s, the rod is non-uniform, so that the Hamiltonian is explicitly s-dependent, and is therefore not an integral. Nevertheless, a tenth integral is still provided by the quantity

$$\mathbf{n} \cdot \mathbf{d}_3 + \frac{|\mathbf{m}|^2}{2\,K_1}\,. \tag{3.45}$$

Rods for which (3.45) is an integral will be described as *uniformly isotropic*, which is a slightly more general case than that of a rod that is both uniform and isotropic.

In summary the Hamiltonian system always has at least eight integrals, namely $\mathbf{n}, |\mathbf{q}|^2, \mathbf{m}+\mathbf{r}\times\mathbf{n}$ and $\boldsymbol{\mu}\cdot\mathbf{q}+2\mathbf{r}\cdot\mathbf{n}$. If the rod is isotropic m_3 provides an additional integral, and if the rod is uniformly isotropic (3.45) provides a tenth integral. Of these ten integrals, all are quadratic functions of the phase variables except (3.45) which is a quartic function. It is straightforward to verify that the gradients of all ten integrals are linearly independent.

There is a well developed theory of integrability in Hamiltonian systems of ordinary differential equations. The classic result is that a Hamiltonian system with N degrees of freedom (i.e. $2N$ equations) is completely integrable if there are N linearly independent integrals in involution. Two integrals I_1 and I_2 are said to commute (or to be in involution) if the Poisson bracket $\{I_1, I_2\} \equiv \nabla I_1 \cdot \mathbf{J}\nabla I_2$ vanishes identically. All N integrals are in involution if all their Poisson brackets vanish identically. We have already shown that there are always eight linearly independent integrals for our seven degree of freedom Hamiltonian system, and that the symmetries of an isotropic, and of a uniformly isotropic rod add a ninth and tenth linearly independent integral. A lengthy, but straightforward, calculation (which, because our integrals are all simple polynomials, can be efficiently carried out by a symbolic manipulation package) reveals that of the eight integrals only five commute, but that of the ten integrals, seven commute.

Thus uniformly isotropic rods represent the only (known) case of complete integrability.

One of the main consequences of complete integrability is the conclusion that there is a choice of coordinates (usually not defined constructively) in which the initial value problem can in principle be completely solved by quadrature. In the case of a uniform, isotropic, twist–free elastica (and using Euler angles rather than Euler parameters to parameterize $SO(3)$) the appropriate calculations are carried out in §19 of [21]. The twisted integrable case and many more calculations are considered in [17] (see also [36] and [35]). The key step is to use cylindrical coordinates to describe the axis of the rod, with the centerline of the cylinder aligned with the direction of the shear force. The explicit coordinates for integration of the rod equilibrium equations were independently rediscovered by Langer and Singer [22] from a very different, rather geometrical point of view, and subsequently detailed calculations were carried out and applied within the context of DNA modelling by Shi and Hearst [34].

It should be understood that a solution by quadrature involves a number of free constants. In an initial value problem, where all the variables are assigned values at $s = 0$, the values of all these constants are typically determined, so that the quadrature is indeed a closed form solution. Initial value problems naturally arise in classic applications of finite dimensional Hamiltonian systems where the independent variable is time. However in the context of rods the independent variable is arc-length, and a two-point boundary value problem arises naturally. In other words, some variables are assigned values at $s = 0$, and some are assigned values at $s = 1$. For such problems a solution by quadrature is not truly explicit, for the values of at least some of the integration constants cannot typically be determined analytically. Accordingly, we are of the opinion that a solution by quadrature is of rather limited utility in the solution of the associated boundary value problems, and our numerical procedures make no use of them. Moreover, the accurate numerical solution of an initial value problem is so straightforward with contemporary machines and software packages, that the use of the solution by quadrature is typically not even an efficient way to numerically generate solutions. In particular, details of various packages developed by K.A. Rogers and R.C. Paffenroth with numerics linked to interactive graphics for examining solutions of the initial value problem for rod equilibria can be found at the World Wide Web URL http://www.glue.umd.edu/~karogers/slinky.html .

4 A Simple Boundary Value Problem

In this section we describe computations of the branches of solutions of the Hamiltonian system (3.40) describing equilibria of the elastica, but within the context of a comparatively simple boundary boundary value problem. The boundary conditions we take correspond to a strut, i.e. a rod that is clamped at one end, and loaded with a prescribed force at the other. The example is chosen because explicit solutions are known for both trivial and non–trivial solution branches, in both isotropic, and non–isotropic cases. Computations with this example allow us to verify both our analytic formulation and the performance of the numerical code. In particular we confirm that our computations achieve various predicted convergence rates, and it is verified that the discretization is sensitive enough to locate secondary bifurcation points on branches of non–trivial equilibria. Most importantly, as described in Subsections 4.5 and 4.6, this simple example allows us to introduce, and numerically test, our procedures for computing representatives of non–isolated solution families, and for breaking continuous symmetries.

4.1 The Strut Boundary Value Problem

Consider the equilibria of a uniform, linearly elastic rod having a rectangular cross section, so that $K_1 \neq K_2$, and a straight, prismatic unstressed state, so that $\hat{\mathrm{u}} \equiv 0$. We assume that the strut is clamped at the end $s = 0$, with the only load acting at the end $s = 1$ being a force of magnitude λ acting anti–parallel to the axis of the undeformed elastica (cf. Fig. 4.1).

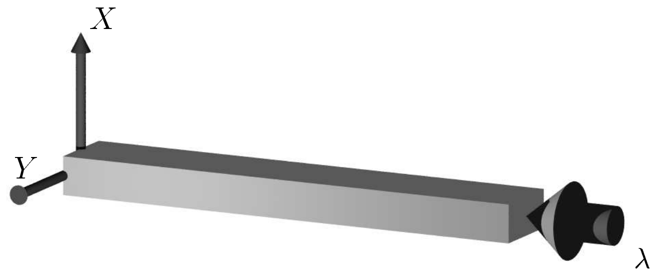

FIGURE 4.1 Schematic of the strut boundary value problem.

The equilibria of the strut are governed by the nonlinear boundary value problem (or BVP) comprising the fourteen differential equations (3.40) described in the previous section (in the linearly elastic case and with $\hat{\mathrm{u}} \equiv 0$), and the boundary conditions

$$
\begin{cases}
\mathbf{r}(0) = (0,0,0), \\
\mathbf{q}(0) = (0,0,0,1), \\
\mathbf{n}(1) = (0,0,-\lambda), \\
(\boldsymbol{\mu}\cdot\mathbf{F}_1\mathbf{q},\ \boldsymbol{\mu}\cdot\mathbf{F}_2\mathbf{q},\ \boldsymbol{\mu}\cdot\mathbf{F}_3\mathbf{q})(1) = (0,0,0), \\
\mu_4(0) = 0.
\end{cases}
\tag{4.1}
$$

The first set of boundary conditions determine the location of the end–point $\mathbf{r}(0)$, the second set fix the orientation of the director basis $\{\mathbf{d}_i(0)\}$, the third specify the force loading, from (3.41) it can be seen that the fourth set prohibit any applied bending moment at the free end, and the final boundary condition eliminates the gauge freedom in the variable $\boldsymbol{\mu}$ that was discussed in Section 3.3.

4.2 Trivial Solutions and Bifurcation Points

As is well–known, for any loading force λ there is a trivial solution of the non–isotropic strut BVP in which the axis remains straight. It is also well–known that there are two sequences of simple bifurcation points on the trivial solution, at which planar equilibria bifurcate, with the deformation either being in the plane of minimum or maximum bending stiffness. We here indicate how to derive closed form formulas for these bifurcation points in terms of the phase variables of our Hamiltonian formulation.

The trivial solution branch can be parameterized by λ in the form

$$
\begin{cases}
\mathbf{r}(s) = (0,0,s), \qquad \mathbf{q}(s) = (0,0,0,1), \\
\mathbf{n}(s) = (0,0,-\lambda), \qquad \boldsymbol{\mu}(s) = (0,0,0,2\lambda s)\ .
\end{cases}
\tag{4.2}
$$

In particular the trivial equilibrium is explicitly s–dependent in the impetus variable $\boldsymbol{\mu}$, which fact necessitates some care in the bifurcation analysis. To find the bifurcation points, we consider perturbations $\mathbf{r}+\delta\,\mathbf{r}, \mathbf{q}+\delta\mathbf{q}, \mathbf{n}+\delta\mathbf{n}, \boldsymbol{\mu}+\delta\boldsymbol{\mu}$ of the trivial solution (4.2) and calculate the linearized version of the BVP. The system so obtained is not constant coefficient, but under the following transformation of the linearized variables, the system becomes constant coefficient:

$$
\delta\tilde{\mathbf{q}} = \sum_{i=1}^{4} \delta q_i \mathbf{B}_i \mathbf{q} \quad , \qquad \delta\tilde{\boldsymbol{\mu}} = \sum_{i=1}^{4} \delta\mu_i \mathbf{B}_i \mathbf{q} \quad .
$$

Here the matrixes $\mathbf{B}_1$, $\mathbf{B}_2$ and $\mathbf{B}_3$ were defined in Section 3.1 and $\mathbf{B}_4$ denotes the 4×4 identity matrix. Accordingly the general solution of the linearized system can be found explicitly, and the determination of the bifurcation points is reduced to finding a solution that satisfies the boundary conditions. We obtain a 14×14 homogeneous system to be solved for the fourteen coefficients arising in the general solution. Accordingly bifurcation points only arise when the coefficient matrix is singular. The appropriate determinant is found to be of the form

$$D = -16\lambda\sqrt{(K_1\,K_2)^3}K_3 \cos\left(\frac{\sqrt{\lambda}}{\sqrt{K_1}}\right)\cos\left(\frac{\sqrt{\lambda}}{\sqrt{K_2}}\right),$$

so that (in the absence of resonances between K_1 and K_2) there are two distinct sequences of simple bifurcation points at the loads

$$\lambda = K_1\left(\frac{\pi}{2}+k\pi\right)^2, \quad \text{and} \quad \lambda = K_2\left(\frac{\pi}{2}+k\pi\right)^2, \quad k = 0, 1, 2, \cdots . \tag{4.3}$$

(It is easy to verify that $\lambda = 0$ is not a bifurcation point.) It should be remarked that for the strut problem, the bifurcation analysis as presented here in terms of the linearized Hamiltonian variables is unduly complicated. However the analysis has exactly the same structure as that required in the more complicated problem of loop buckling that we examine in Section 5.2. Moreover our formulation is well–suited to treatment using symbolic manipulation packages.

4.3 Numerical Methods

We applied the numerical continuation code AUTO [10] to follow the solution branches emanating from these bifurcation points (4.3). The AUTO software package is designed for continuation and bifurcation problems in ordinary differential equations using a collocation method for discretization. AUTO is capable of solving parameterized first order systems of ordinary differential equations in the form

$$\mathbf{u}'(s) = \mathbf{f}(\mathbf{u}(s), \boldsymbol{\lambda}), \quad s \in [0,1], \quad \mathbf{u}(\cdot), \mathbf{f}(\cdot,\cdot) \in \mathbb{R}^{\mathrm{n}}, \quad \boldsymbol{\lambda} \in \mathbb{R}^{\mathrm{n}_\lambda}, \tag{4.4}$$

subject to general, possibly nonlinear or non–separated, boundary conditions

$$G_i(\mathbf{u}(0), \mathbf{u}(1), \boldsymbol{\lambda}) = 0, \qquad i = 1, 2, \cdots, n_b\,. \tag{4.5}$$

Here $\boldsymbol{\lambda}$ is a vector of parameters. In order for problem (4.4)—(4.5) to be formally well–posed it is required that the numbers of parameters, boundary conditions and equations are related through the equation $n_\lambda = n_b - n + 1$, which implies that there will always be one free parameter so that the equations can be expected to yield curves of solutions, i.e. we are concerned with a one parameter continuation problem. In particular, for the strut problem we have $n = 14$, $n_b = 14$ and one continuation parameter $n_\lambda = 1$.

The details of the numerical procedures used in AUTO can be found in Doedel et al. [11], [12]. There is an extensive literature concerning error analyses of collocation methods (see, for example, [2], [5], [15] and [30]). Here we merely mention the following three error estimates. Assuming that the problem (4.4)—(4.5) is sufficiently smooth, the local behavior of the error for the mesh interval $s \in [s_i, s_{i+1})$ is

$$\|u_l(s) - v_l(s)\|_{(i)} = c_l |u_l^{m+1}(s_i)| h_i^m + O(h_i^{m+1}), \quad l = 1, 2, \cdots, n,$$

where $h_i = s_{i+1} - s_i$, and c_l are known constants, m is the number of collocation points on each of N mesh intervals, $u_l(s)$ and $v_l(s)$ denote the n components of respectively the exact and collocation solutions, and for any appropriate function ψ, the local norm $\|\psi\|_{(i)}$ is defined by

$$\|\psi\|_{(i)} := \max_{s \in [s_i, s_{i+1})} |\psi(s)|.$$

If the mesh is uniform,

$$\|u_l(s) - v_l(s)\|_{L^\infty([0,1])} = O(h^{m+1}),$$

and at mesh points s_i there is super-convergence

$$\max_{0 \le i \le N} |u_l(s_i) - v_l(s_i)| = O(h^{2m}), \quad l = 1, 2, \cdots, n.$$

4.4 Bifurcation Diagrams and Computational Results

We first used AUTO to compute buckled modes of the strut BVP. Starting from a point on the trivial solution branch, AUTO readily identified the simple bifurcation points given by the formula (4.3) lying within the specified search range. Switching to the nontrivial branches was similarly robust, and the code was also able to detect secondary bifurcation points on some of the higher mode primary branches. (The presence of such secondary bifurcations is forced by the possibility of multiple bifurcation points arising from equal buckling loads associated with different values of the integer k in the two sequences (4.3), however the details are not pertinent here.)

For this simple problem, the primary bifurcation branches involve planar equilibria, with an explicit closed form solution in terms of elliptic integrals and functions. For example, the centerline of the strut on the first primary bifurcation branch is given by

$$\begin{cases} x = 0\,, \\[2ex] y = 2k\sqrt{\dfrac{K_1}{\lambda}}\left(1 - \mathrm{cn}\left(\sqrt{\dfrac{\lambda}{K_1}}s, k\right)\right)\,, \\[2ex] z = \sqrt{\dfrac{K_1}{\lambda}}\left(2\mathrm{E}\left(\mathrm{am}\sqrt{\dfrac{\lambda}{K_1}}s, k\right) - \sqrt{\dfrac{\lambda}{K_1}}s\right)\,, \end{cases}$$

where $k = \sin(\alpha/2)$ and α is the angle between the z–axis and the tangent direction of the strut at the free end. Using this explicit solution, we are able to verify that the errors and convergence rates of the numerical solutions are in accordance with theoretical predictions (cf. Figures 4.2 and 4.3).

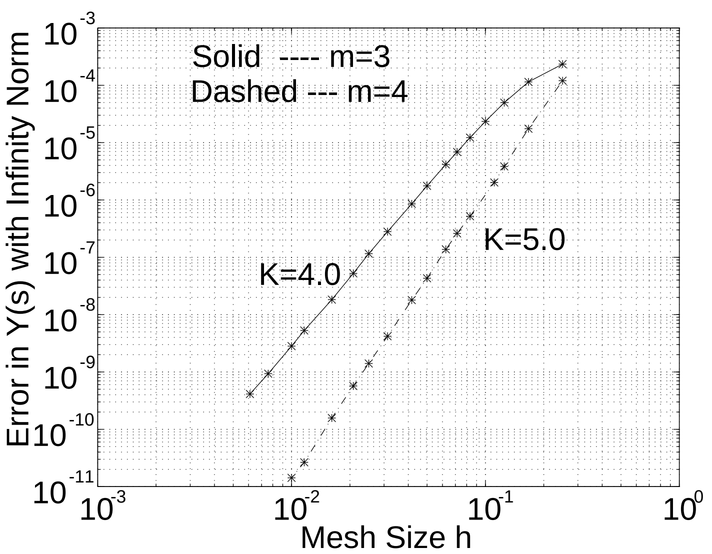

FIG. 4.2 *Convergence rate of the error in the component $y(s)$ of the solution measured in the L^∞ norm. Here m denotes the degree of polynomial used on each subinterval, and the slope K is the convergence rate.*

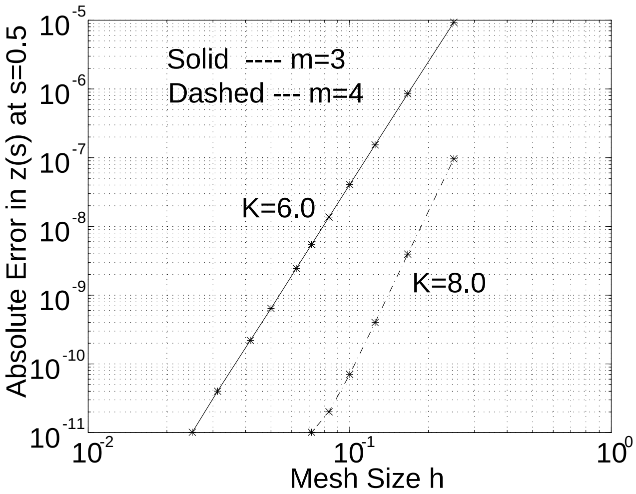

FIG. 4.3 *Super–convergence rate of the absolute error in the component $z(s)$ at the mesh point $s = 0.5$. Here m denotes the degree of polynomial used on each subinterval, and the slope K is the convergence rate.*

4.5 The Isotropic Strut

In the limit $K_1 \to K_2$ we obtain an isotropic rod, and the two (generically) distinct sequences of simple bifurcation points coalesce into a single sequence of double bifurcation points. The strut BVP is sufficiently simple that there is no associated difficulty in the analysis. At each double bifurcation point a two-dimensional paraboloid sheet of non-planar equilibria arises. At fixed load λ, each nontrivial equilibrium is an element of a circle of equilibria in the bifurcation surface. All the equilibria in this one-parameter family are generated from any other by a composite continuous symmetry. The symmetry is generated by a rigid body rotation about the Z–axis, which violates the boundary conditions on the directors at $s = 0$, coupled with an s–dependent rotation in which the rod is spun about its own centerline in such a way as to correct the boundary conditions on the directors at $s = 0$.

The presence of this one parameter family of solutions to the BVP at fixed load is incompatible with simple numerical continuation procedures, which require that solutions be locally isolated for fixed parameter values (at other than exceptional points). The problem can be overcome by adding boundary conditions or other side conditions, that factor out the symmetry by picking specific representatives of the symmetry generated solution family. For example, the boundary condition

$$\mathbf{d}_3(1) \cdot (\mathbf{i} + \mathbf{j}) = 0 \tag{4.6}$$

selects two representatives, lying in the plane $X + Y = 0$, from each of the symmetry generated families of nontrivial solutions. Furthermore, and with the possible exception of a small number of secondary bifurcation points, the $X + Y = 0$ equilibria form branches of solutions that are locally isolated at fixed λ. Of course we could select different locally isolated representatives of the symmetric solution family by prescribing other components of $\mathbf{d}_3(1)$ to vanish.

We are then presented with a BVP that is, *a priori*, over-determined. Properly chosen additional boundary conditions pose no difficulty in analysis because, by construction, any necessary solvability conditions are satisfied by dint of the continuous symmetry. However, for numerical procedures the disparity in the count between the numbers of boundary conditions and equations is a significant difficulty. In particular for one parameter continuation, the AUTO code requires that the number of imposed boundary conditions equals the number of unknown functions. So, for example, with the Hamiltonian system (3.40), we can only impose fourteen boundary conditions.

The difficulties with over-determinacy could perhaps be addressed by modifications to the numerical discretization. Here we instead describe an explicit modification of the continuous BVP that allows an unmodified discretization and numerical procedure to be applied. The difficulty of non-isolation is caused by the presence of a continuous symmetry. For problems with a variational structure (in either Lagrangian or Hamiltonian form) Noether's Theorem states that the presence of a (variational) continuous symmetry, implies the existence of an associated integral. (In the examples of concern here, both the symmetry and the invariant are known explicitly, so we shall not pause to make the general claim precise.) For the strut BVP, the non-isolation only arises in the case of isotropy, with the associated symmetry being rotation about the centerline of the rod. The additional integral associated with isotropy is the twist $m_3(s)$. Integrals serve to carry information from $s = 0$ to $s = 1$. Consequently in the case of isotropy some boundary conditions at $s = 1$, say, may actually be implied by others at $s = 1$ taken in combination with those at $s = 0$. This is the outline of the method for modifying boundary conditions that we shall now make explicit in the particular context of the BVP for the isotropic strut.

Consider the Hamiltonian BVP comprising equations (3.40) subject to the fourteen boundary conditions

$$\begin{cases} \mathbf{r}(0) = (0,0,0), \quad \mathbf{q}(0) = (0,0,0,1), \\ \mathbf{n}(1) = (0,0,-\lambda), \quad \mu_4(0) = 0, \\ \mathbf{m}(1)\cdot(\mathbf{i}+\mathbf{j}) = 0, \quad \mathbf{m}(1)\cdot\mathbf{k} = 0, \\ \mathbf{d}_3(1)\cdot(\mathbf{i}+\mathbf{j}) = 0. \end{cases} \tag{4.7}$$

In particular these boundary conditions do not *a priori* imply that the moment $\mathbf{m}(1)$ vanish, as required by boundary conditions (4.1), but only that the two components in the directions $\mathbf{k}$ and $\mathbf{i}+\mathbf{j}$ vanish.

It is simple to verify that the trivial branch of solutions satisfies both boundary conditions (4.1) and (4.7). Moreover, at fixed λ the $X+Y=0$, non-trivial solutions of (4.1) are locally isolated solutions to the set of fifteen boundary conditions (4.1) and (4.6). The solutions are locally isolated because, by construction, the fifteenth boundary condition (4.6) selects two representatives from the circle of symmetry related configurations. It is also clear that the the $X+Y=0$, non-trivial solutions of (4.1) necessarily satisfy the set of fourteen boundary conditions (4.7). We further claim that they are *locally isolated when regarded as solutions to* (4.7). To prove this fact, it suffices to demonstrate that any solution of the fourteen boundary conditions (4.7) lying close to a nontrivial solution of (4.1), actually satisfies $\mathbf{m}(1) = \mathbf{0}$, so that it is also solution of the fifteen boundary conditions (4.1) and (4.6), and is therefore locally isolated. Notice that we do not claim that all solutions satisfying (4.7) necessarily satisfy (4.1) and (4.6). Indeed it turns out that there are equilibria satisfying (4.7) with $\mathbf{d}_3(1)$ parallel to $\mathbf{k}$ that do *not* satisfy (4.1). We refer to these configurations as spurious solutions. The point is that these spurious solutions cannot be close to non-trivial solutions of (4.1), and therefore do not give rise to any difficulty.

Explicitly, we argue that whenever $\mathbf{d}_3(1)$ is not parallel to $\mathbf{k}$, which is always true on the non-trivial solution branches of (4.1), then indeed $\mathbf{m}(1) = \mathbf{0}$ as required. With isotropy, $m_3(s)$ is an integral, i.e.

$$\mathbf{m}(1)\cdot\mathbf{d}_3(1) = \mathbf{m}(0)\cdot\mathbf{d}_3(0)\,.$$

Hence, because $\mathbf{d}_3(0) = \mathbf{k}$ for the strut,

$$\mathbf{m}(1)\cdot\mathbf{d}_3(1) = \mathbf{m}(0)\cdot\mathbf{k}\,.$$

On the other hand, because $\mathbf{n}\times\mathbf{k} = \mathbf{0}$ we find from the integral

$$\mathbf{m}(s) + \mathbf{r}(s)\times\mathbf{n}(s) = \mathbf{m}(0),$$

that

$$\mathbf{m}(1) \cdot \mathbf{k} = \mathbf{m}(0) \cdot \mathbf{k}\,.$$

Consequently the boundary condition $\mathbf{m}(1)\cdot\mathbf{k} = 0$ implies that $\mathbf{m}(1)\cdot\mathbf{d}_3(1) = 0$. By boundary condition (4.6), and the assumption $\mathbf{d}_3(1) \times \mathbf{k} \neq \mathbf{0}$, the triple $\{\mathbf{d}_3(1),\ (\mathbf{i}+\mathbf{j}),\ \mathbf{k}\}$ forms a basis; accordingly, since $\mathbf{m}(1) \cdot \mathbf{d}_3(1) = \mathbf{m}(1) \cdot (\mathbf{i}+\mathbf{j}) = \mathbf{m}(1) \cdot \mathbf{k} = 0$, we have $\mathbf{m}(1) = \mathbf{0}$ as required.

Notice that the above argument does *not* imply that all solutions of (4.7) in the neighborhood of the trivial branch are also solutions of (4.1), because $\mathbf{d}_3(1) = \mathbf{k}$ on the trivial branch . And indeed, a bifurcation analysis of the trivial solution to (3.40) subject to the boundary conditions (4.7) reveals that there are two, strictly interlaced, sequences of simple bifurcation points. One sequence corresponds to the desired isolated representatives of the solutions of the BVP with boundary conditions (4.1), and the other to bifurcating branches of spurious nontrivial solutions along which $\mathbf{d}_3(1) = \mathbf{k}$ and $\mathbf{m}(1) \neq \mathbf{0}$. The branches of spurious solutions do not interfere with the desired computations because they are readily identified and ignored. Locally isolated solutions satisfying (4.7) are readily computed using AUTO starting from the trivial branch. The branch of nontrivial solutions colored green in Figure 4.4 was computed this way. (Color figures appear at the end of the article.)

4.6 Symmetry Breaking

The final computation that we performed with the strut BVP is to break isotropic symmetry, to compute solutions to certain imperfect problems. The objective is to obtain a single solution on as many connected components of the perturbed solution set as possible. After that goal is achieved the problem is reduced to a standard one of continuation from a known starting point using the load parameter λ and the non–symmetric BVP comprising equations (3.40) and boundary conditions (4.1).

For given load parameter λ it can certainly be anticipated that for small imperfections solutions of the perturbed problem will lie close to the non-isolated families of solutions to the symmetric BVP. But it need not be true that solutions to the perturbed problem lie close to the particular representatives of the family of symmetric solutions that are singled out by boundary conditions (4.7) in the computational procedure described in the previous section. That is why some care is needed in numerically breaking symmetry. For the particular case of the strut, the computations we describe are actually unnecessary because matters can be arranged so that each connected component of equilibria of the perturbed problem passes close to the isolated, trivial solution of the perfect problem, and it is quite simple to perturb from there. However, for the loop BVP that we will discuss next, it is necessary to perturb from a one-parameter family of non-isolated, symmetry related solutions, so we first test our numerical procedure for that harder task in the context of the comparatively simple strut BVP.

The test problem we consider is the computation of equilibria of a non–isotropic strut in which the unstressed centerline is curved, and the two bending stiffnesses are distinct. To achieve this we introduce a homotopy parameter in the coefficient functions appearing in (3.40). Specifically we consider a family of bending stiffnesses

$$K_1(\gamma) = K_1, \qquad K_2(\gamma) = K_1 + \gamma(K_2 - K_1)\,, \tag{4.8}$$

and unstressed curvatures

$$\hat{\mathsf{u}}(\gamma) = (\gamma\hat{u}_1, \gamma\hat{u}_2, 0). \tag{4.9}$$

With $\gamma = 0$ the isotropic problem arises, and with $\gamma = 1$ we have the desired coefficients for our non-isotropic imperfect problem.

We base our procedure on the following observation. With λ held fixed at a prescribed value, equations (3.40) with coefficients (4.8) and (4.9) subject to boundary conditions (4.1) comprise a well-defined continuation problem in the single parameter γ. The problem has a one-dimensional symmetry-related family of otherwise isolated solutions on which $\gamma \equiv 0$. The family is generated by the action of the same continuous symmetry of composite rotations that implied non-isolation of the symmetric strut (as described in the previous Subsection). This $\gamma \equiv 0$, symmetry-related family is nontrivial, i.e. involves different equilibria, whenever a buckled equilibrium is under consideration. Solutions in the symmetry related family that lie close to solutions of the imperfect problem are singled out as bifurcation points at which it is possible to switch to branches of solutions with $\gamma \neq 0$.

Our experience with AUTO is that the code can robustly follow the curve of $\gamma = 0$ solutions. This is in part because AUTO uses pseudo-arclength continuation in order to be able to traverse fold points at which the continuation parameter passes through a local extremum. In our context we specify γ as the continuation parameter, and γ happens to be exactly constant all along the curve of symmetry-related equilibria. In the examples that we considered, this fact presented no numerical difficulties for AUTO. As depicted in the circular orange segment of Figure 4.4, when we started continuation in γ from an $X + Y = 0$ equilibrium, AUTO produced a sequence of solutions traversing the symmetry-generated branch. Points along the circular branch at which γ could be made nonzero were also detected and reported as bifurcation points. For the perturbations detailed here, the number of bifurcation points was typically found to be four. But there were some cases of only two bifurcation points, particularly when $K_2 = K_1$ so that isotropy was broken only by unstressed curvatures, and not by differing bending stiffnesses. At these bifurcation points, the continuation procedure can switch branches and the new, imperfect path traversed until the value $\gamma = 1$ of the imperfection parameter is reached. These four segments are shown in red in Figure 4.4, but are rather short, and two of these branches are completely obscured in the Figure. Finally the desired connected components of the perturbed bifurcation set were found by maintaining $\gamma = 1$, and switching back to continuation in λ. These branches are shown in blue in Figure 4.4.

We remark that the procedure described here hinges on the fact that the symmetry-related $\gamma \equiv 0$ family of solutions is one-dimensional. At some solutions of the loop BVP that are described in the next section, the symmetry generated family is two-dimensional, and our procedures must be modified accordingly.

5 The Uniformly Isotropic Loop

We now apply the machinery developed in the previous Sections to the boundary value problem of primary interest, namely that in which a rod is bent into a loop and then closed upon itself after being subjected to a prescribed twist (or linking difference). In this section we concentrate on the integrable case of a uniformly isotropic rod, and we compute the rather intricate bifurcation set of this highly-symmetric problem. In Section 6 this perfect solution set is exploited as an organizing center for the computation of the solution set for various imperfect, non-integrable cases using our symmetry-breaking techniques.

In Subsection 5.1 a BVP that governs the equilibria of the loop is developed. In particular we describe boundary conditions for a uniformly isotropic loop that give rise to branches of locally isolated representatives of symmetry-related non-isolated solutions. In Subsection 5.2, families of 'trivial' closed form solutions comprising singly- and multiply-covered twisted circles are described, and a bifurcation analysis based on Euler parameters is made. In Subsection 5.3, numerical computations of branches of non-planar solutions are presented. and intricate patterns of connectivity, nodal properties, and self–intersection are revealed.

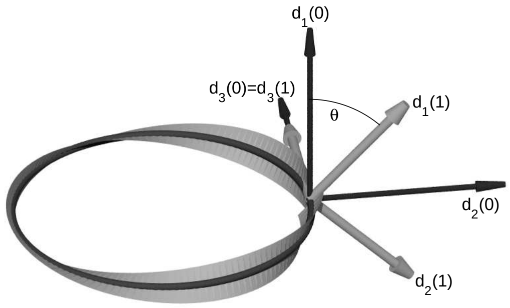

FIG. 5.1 *Schematic of the boundary value problem for a closed, twisted rod.*

5.1 The Boundary Value Problem for the Loop

As before, the equilibrium equations governing the loop are the system of fourteen first–order nonlinear differential equations (3.40). For the closed, twisted loop depicted in Figure 5.1, an appropriate set of fourteen boundary conditions is

$$\mathbf{r}(0) = \mathbf{r}(1) = (0,\, 0,\, 0), \tag{5.1}$$

$$(q_1(0),\, q_2(0),\, q_3(0)) = (0,\, 0,\, 0), \tag{5.2}$$

$$\mathbf{q}(1) = (0,\, 0,\, -\sin(\theta/2),\, -\cos(\theta/2)), \tag{5.3}$$

$$\mu_4(0) = 0. \tag{5.4}$$

Here (5.1) implies that the centerline of the rod closes upon itself, and that the two end points are fixed at the origin (which factors out the symmetry of rigid body translations in space). Consideration of the expressions (3.15) and (3.16) for the directors in terms of the Euler parameters reveals that equation (5.2) specifies the orientation of the director triad $\mathbf{d}_i(0)$ to coincide with the standard fixed basis (which can be regarded as eliminating the symmetry of overall rigid body rotations). Similarly, the boundary condition (5.3) completely specifies the orientation of the director triad $\mathbf{d}_i(1)$ to be such that the tangents to the centerline of the rod close smoothly, i.e. $\mathbf{d}_3(1) = \mathbf{d}_3(0) = \mathbf{k}$, and there is an imposed angle θ between the vectors $\mathbf{d}_1(0)$ and $\mathbf{d}_1(1)$. The angle θ will serve as the loading and continuation parameter in our computations. It should also be remarked that the boundary condition $q_4(0) = 1$ need not be explicitly prescribed, for the integral $|\mathbf{q}|^2$ implies that $|\mathbf{q}(0)|^2 = |\mathbf{q}(1)|^2 = 1$, by boundary conditions (5.3). Accordingly, with boundary conditions (5.2), if $q_4(0) = +1$ at a starting configuration the same value is enforced on the entire connected component of the solution set. As will be seen from the closed form solutions presented in the next Subsection, the choice of signs appearing in (5.3) turns out to be natural because of the double covering of $SO(3)$ provided by the Euler parameters $\mathbf{q}$. Finally equation (5.4) uniquely determines the value of the integral $\boldsymbol{\mu} \cdot \mathbf{q} + 2\mathbf{r} \cdot \mathbf{n}$, and eliminates the gauge freedom in the variable $\boldsymbol{\mu}$ that was described in Section 3.3.

The count for equations (3.40) subject to boundary conditions (5.1)–(5.4) is formally correct—fourteen equations, fourteen boundary conditions, and a single continuation parameter θ. It can therefore be anticipated that varying θ should generate a one-dimensional family of locally isolated equilibria. Our computations of non-symmetric rods that are described in Section 6 confirm this conjecture, but for such rods there is no known closed-form solution to use as a starting point for numerical continuation. In the next Subsection we display closed-form solutions for the integrable case of a uniform, isotropic rod, that *can* serve as starting points for numerical continuation. However for such symmetric rods the boundary conditions (5.1)–(5.4) do not yield locally isolated solutions. This non-isolation, and a set of modified boundary conditions that eliminate it, are the subject of discussion in the remainder of this Subsection.

A uniform, isotropic rod has two constitutive-dependent continuous symmetries in addition to the constitutive-independent rigid-body symmetries. The additional symmetries are translation in arc-length, and rotations of the director basis about the tangent $\mathbf{d}_3(s)$. Each of these symmetries leads to non-isolation of equilibria. Notice that unless the centerline of the configuration is straight, spinning the rod about its own centerline is not equivalent to a rigid body rotation.

Just as for the strut BVP, the non-isolation for isotropic rods is generated by a composite symmetry in which a rigid body rotation about the $\mathbf{k}$ axis is coupled with a rotation of the directors about the rod centerline. The rigid body rotation will lead to violation of boundary conditions (5.2) and (5.3), but the rotation about the centerline can be chosen such that the composition does satisfy (5.2) and (5.3). The only fixed points of this continuous symmetry group are straight rods, which are not possible configurations with boundary conditions (5.1)—(5.4), so isotropy will always create non-isolation. The force $\mathbf{n}$ is rotated by the symmetry, so it is apparent that unless $\mathbf{n}$ is tangent to the rod at the origin (which is not the case on the solutions of interest to us here), the additional boundary condition

$$n_2(0) = 0, \tag{5.5}$$

will select two locally-isolated representatives of the family of solutions generated by isotropy.

For uniform rods, the symmetry of translation in arc-length for equations (3.40) is a symmetry of the BVP with boundary conditions (5.1)—(5.4) when the frames $\{\mathbf{d}_i(0)\}$ and $\{\mathbf{d}_i(1)\}$ are fully aligned, i.e. $\theta = 2n\pi$. Then both the centerline $\mathbf{r}(s)$ and the frame $\{\mathbf{d}_i(s)\}$ can be regarded as periodic functions of period 1, and solutions can be generated by shifts in arc–length, coupled with rigid body motions to correct boundary conditions (5.1)—(5.2). Since the centerline of the rod is closed, and the force $\mathbf{n}$ is constant, the quantity $\mathbf{d}_3(s) \cdot \mathbf{n} = \mathbf{r}' \cdot \mathbf{n}$ must vanish at two or more points; by using translational invariance we may therefore specify that

$$\mathbf{n} \cdot \mathbf{k} = \mathbf{n} \cdot \mathbf{d}_3(0) = n_3(0) = 0. \tag{5.6}$$

The addition of boundary condition (5.6) will select isolated representatives of the symmetry generated family of solutions, unless $n_3(s)$ vanishes on a range of s values. As it happens, this case does arise, but only when $n_3(s)$ vanishes identically, and the equilibria involve circular centerlines that are fixed points of the symmetry group. Consequently boundary condition (5.6) can always be prescribed, and it serves to eliminate non-isolation associated with the symmetry of uniformity.

The integrable case of uniform, isotropic rods is of particular concern. For such rods it can be shown that the symmetry of translation in s can be used to generate other solutions of the BVP even if the frame $\{\mathbf{d}_i(s)\}$ is not periodic, i.e. $\theta \neq 2n\pi$. The required argument exploits a coupling between translational invariance and the properties of isotropy as described in Section 3.3. Consequently, any equilibrium of an integrable rod that does not have a circular centerline is embedded in a two–torus of solutions generated by the two symmetries. The equilibria with circular centerlines are embedded in only a one–torus (or circle) of solutions generated by isotropy, for they are fixed points of translational invariance which generates the second dimension for non-circular equilibria. The equilibria of a uniform, isotropic rod that have circular centerlines are precisely the closed form solutions that are detailed in the next Subsection. On these solutions $\mathbf{n} \cdot \mathbf{d}_3(s) \equiv 0$. Consequently, it is still possible to simultaneously prescribe both boundary conditions (5.5) and (5.6), and locally isolated equilibria are thereby obtained. A much more detailed and comprehensive discussion of the symmetry properties of the closed elastic loop has been made by Domokos [14].

Just as in the strut example, we cannot merely add boundary conditions (5.5) and (5.6) to factor out the symmetry-induced non-isolation and still hope to apply standard numerical continuation techniques, because there would then be a disparity between the numbers of boundary conditions, equations and parameters. As before, the resolution is to exploit the additional integrals generated by the symmetries to show that some boundary conditions are actually implied, and so need not be enforced. Explicitly, we claim that for a uniformly isotropic rod the following fourteen boundary conditions lead to locally isolated solutions of the ring BVP (5.1)–(5.4):

$$\mathbf{r}(0) = \mathbf{r}(1) = (0,\, 0,\, 0), \tag{5.7}$$

$$(q_1(0),\, q_2(0),\, q_3(0)) = (0,\, 0,\, 0), \tag{5.8}$$

$$q_3(1) = -\sin(\theta/2), \qquad q_4(1) = -\cos(\theta/2), \tag{5.9}$$

$$\mu_4(0) = 0, \qquad n_2(0) = 0, \qquad n_3(0) = 0\,. \tag{5.10}$$

In particular the missing boundary conditions $q_1(1) = 0$ and $q_2(1) = 0$ are implied by (5.7)–(5.10), provided that the rod is uniformly isotropic. To see this fact we argue as follows. For a uniformly isotropic rod (3.45) is an integral, so that

$$\mathbf{n}\cdot\mathbf{d}_3(0) + \frac{|\mathbf{m}(0)|^2}{2\,K_1} = \mathbf{n}\cdot\mathbf{d}_3(1) + \frac{|\mathbf{m}(1)|^2}{2\,K_1}. \tag{5.11}$$

From the integral $\mathbf{m} + \mathbf{r}\times\mathbf{n}$, and boundary condition (5.7), we may also conclude

$$\mathbf{m}(0) = \mathbf{m}(1), \tag{5.12}$$

so that equation (5.11), taken with boundary conditions (5.6) and (5.8), implies that

$$\mathbf{n}\cdot\mathbf{d}_3(1) = \mathbf{n}\cdot\mathbf{d}_3(0) = \mathbf{n}\cdot\mathbf{X} = 0, \tag{5.13}$$

i.e., the vector $\mathbf{d}_3(1)$ lies in the Y–Z plane. On the other hand, we have from equation (5.12) and the twist integral m_3 that

$$\mathbf{m}(0)\cdot\mathbf{d}_3(1) = \mathbf{m}(1)\cdot\mathbf{d}_3(1) = m_3 = \mathbf{m}(0)\cdot\mathbf{d}_3(0). \tag{5.14}$$

Equations (5.13) and (5.14) are two coupled equations for the unknown unit vector $\mathbf{d}_3(1)$, expressing the fact that the vector $\mathbf{d}_3(1)$ lies in the intersection of the plane orthogonal to $\mathbf{n}$ and a right circular cone with axis $\mathbf{m}(0)$. Moreover, one solution of this quadratic set of equations is $\mathbf{d}_3(1) = \mathbf{d}_3(0)$, or equivalently $q_1(1) = q_2(1) = 0$ as desired. As one solution of the system is known, in the generic case the cone and the plane intersect in two distinct directions. It may accordingly be concluded that if connected branches of solutions to boundary conditions (5.7)–(5.10) are computed starting from a configuration at which $\mathbf{d}_3(0) = \mathbf{d}_3(1)$, then locally isolated branches of solutions to boundary conditions (5.1)–(5.4) will be found. There are only two exceptional cases in which some care must be taken, namely $m_3 = 0$ with $\mathbf{m}(0) \times \mathbf{n} = \mathbf{0}$ when the cone degenerates and coincides with the plane, and the case of double roots, when the cone is tangent to the plane. As it happens the first case is of no consequence in our computations. However the case of double roots does arise; in fact, precisely on the trivial solutions described in the next section. Just as in the strut BVP, the double root can split to yield branches of spurious solutions with $\mathbf{d}_3(0) \neq \mathbf{d}_3(1)$, but only at a sequence of explicitly known bifurcation points, and as before no real obstacle to our computations arises.

5.2 Trivial Solutions and Bifurcation Analysis

In this Subsection, we present formulas for the trivial circular solutions of the loop BVP in terms of Euler parameters. An associated bifurcation analysis is also described.

The N covered circles

$$\mathbf{r}(s) = (0, \frac{\cos 2N\pi s - 1}{2N\pi}, \frac{\sin 2N\pi s}{2N\pi}), \tag{5.15}$$

are closed form solutions for the centerline $\mathbf{r}(s)$. Here $N = 1, 2, 3, \cdots$ with N denoting the number of times the rod covers itself. The associated force $\mathbf{n}$ and bending moment $\mathbf{m}(s)$ are

$$\mathbf{n}(s) = (\lambda, 0, 0), \tag{5.16}$$

and

$$\mathbf{m}(s) = (2N\pi, -K_3\omega \sin 2N\pi s, K_3\omega \cos 2N\pi s),$$

where ω is the constant value of the twist rate u_3. From the integral $\mathbf{m}+\mathbf{r}\times\mathbf{n}$, and the boundary condition $\mathbf{r}(0) = \mathbf{0}$, it follows that

$$\mathbf{m}(s) + \mathbf{r}(s) \times \mathbf{n}(s) = \mathbf{m}(0),$$

which yields a correspondence between the shear force λ and the twist rate ω

$$\lambda = 2N\pi K_3\omega. \tag{5.17}$$

The associated Euler parameters $\mathbf{q}$ are

$$\begin{cases} q_1(s) = \sin N\pi s \cos \dfrac{\omega s}{2}, \\ q_2(s) = -\sin N\pi s \sin \dfrac{\omega s}{2}, \\ q_3(s) = \cos N\pi s \sin \dfrac{\omega s}{2}, \\ q_4(s) = \cos N\pi s \cos \dfrac{\omega s}{2}, \end{cases} \tag{5.18}$$

with the ω defined as in (5.17). Finally the solution for $\boldsymbol{\mu}$ is

$$\begin{cases} \mu_1(s) = 4N\pi K_1 \cos N\pi s \cos \dfrac{\omega s}{2} - 2K_3\omega \sin N\pi s \sin \dfrac{\omega s}{2}, \\ \mu_2(s) = -4N\pi K_1 \cos N\pi s \sin \dfrac{\omega s}{2} - 2K_3\omega \sin N\pi s \cos \dfrac{\omega s}{2}, \\ \mu_3(s) = -4N\pi K_1 \sin N\pi s \sin \dfrac{\omega s}{2} + 2K_3\omega \cos N\pi s \cos \dfrac{\omega s}{2}, \\ \mu_4(s) = -4N\pi K_1 \sin N\pi s \cos \dfrac{\omega s}{2} - 2K_3\omega \cos N\pi s \sin \dfrac{\omega s}{2}. \end{cases} \tag{5.19}$$

The BVP has other closed form solutions in which the centerlines are the mirror images of (5.15) in the X-Z plane:

$$\mathbf{r}(s) = (0, \frac{1-\cos 2N\pi s}{2N\pi}, \frac{\sin 2N\pi s}{2N\pi}). \tag{5.20}$$

On these solutions the force λ and the twist rate ω are related by

$$\lambda = -2N\pi K_3\omega\,. \tag{5.21}$$

In consonance with the signs appearing in (5.17) and (5.21), we shall refer to positive and negative twist solutions, although each family has solutions with ω of either sign. Indeed, for prescribed ω the two circular configurations (5.15) and (5.20) with equal but opposite components of force as determined by (5.17) and (5.21) give rise to solutions that serve as two locally isolated representatives of the one-parameter family of solutions to the

BVP with boundary conditions (5.1)–(5.4) that is generated by the symmetry of isotropy.

For the bifurcation analysis, we mimic the procedure introduced in the strut BVP. More details of the analysis are presented elsewhere. Let $\mathbf{z} = (\mathbf{r}, \mathbf{n}, \mathbf{q}, \boldsymbol{\mu})$ denote the trivial solutions (5.15), (5.16), (5.18) and (5.19), and $\delta\mathbf{z} = (\delta\mathbf{r}, \delta\mathbf{n}, \delta\mathbf{q}, \delta\boldsymbol{\mu})$ denote perturbations. Then we seek nontrivial solutions $\delta\mathbf{z}$ satisfying the following system of linearized differential equations:

$$\delta\mathbf{z}' = \mathbf{J}\nabla^2\mathcal{H}(\mathbf{z})\delta\mathbf{z}, \tag{5.22}$$

subject to the linearization of the boundary conditions (5.7)—(5.10). The matrix $\mathbf{M} = \mathbf{J}\nabla^2\mathcal{H}(\mathbf{z})$ so obtained is s dependent. However, under the s-dependent change of variable

$$\delta\tilde{\mathbf{r}} = \mathbf{R}_1^T\delta\,\mathbf{r}, \qquad \delta\tilde{\mathbf{n}} = \mathbf{R}_1^T\delta\,\mathbf{n},$$

with

$$\mathbf{R}_1 = \begin{pmatrix} 1 & 0 & 0 \\ 0 & \cos 2N\pi s & \sin 2N\pi s \\ 0 & -\sin 2N\pi s & \cos 2N\pi s \end{pmatrix},$$

and

$$\begin{cases} \delta\tilde{\mathbf{q}} = \delta q_1\mathbf{C}_1 + \delta q_2\mathbf{C}_2 + \delta q_3\mathbf{B}_3\mathbf{q} + \delta q_4\mathbf{q}, \\ \delta\tilde{\boldsymbol{\mu}} = \delta\mu_1\mathbf{C}_1 + \delta\mu_2\mathbf{C}_2 + \delta\mu_3\mathbf{B}_3\mathbf{q} + \delta\mu_4\mathbf{q} \end{cases}$$

with

$$\mathbf{C}_1 = \cos 2N\pi s\mathbf{B}_1\mathbf{q} + \sin 2N\pi s\mathbf{B}_2\mathbf{q},$$
$$\mathbf{C}_2 = -\sin 2N\pi s\mathbf{B}_1\mathbf{q} + \cos 2N\pi s\mathbf{B}_2\mathbf{q},$$

a constant coefficient system is obtained:

$$\delta\tilde{\mathbf{z}}' = \widetilde{\mathbf{M}}\,\delta\tilde{\mathbf{z}}. \tag{5.23}$$

As before, determination of the bifurcation points is now reduced to finding the roots of a 14×14 determinant which simplifies to

$$\frac{8N^2\pi(k\pi\cos k\pi - \sin k\pi)\sin k\pi}{8k^4N^2\pi^3\sqrt{k^2 - N^2}},$$

where $k = \sqrt{N^2 + \left(\dfrac{\omega K_3}{2\pi K_1}\right)^2}$. Consequently, the determinant vanishes, if $k = 1, 2, \cdots$, or if k is a root of the equation

$$k = \frac{1}{\pi}\tan k\pi. \tag{5.24}$$

However it can be verified that when k is a root of (5.24), $\delta\mathbf{d}_3(0) \neq \delta\mathbf{d}_3(1)$. Therefore, these bifurcation points correspond to spurious branches, and can be ignored.

In summary we have a formula in terms of the twist rate

$$\omega = \pm\, 2\pi \frac{K_1}{K_3}\sqrt{(M+N)^2 - N^2}\,, \qquad M = 1,\, 2, \cdots , \tag{5.25}$$

for the bifurcation points, and it can be verified that bifurcations arise on both the positive and negative twist families for both positive and negative values of ω.

A straightforward computation shows that at the Mth $\omega > 0$ bifurcation point on the N-covered positive-twist circle there are eigenfunctions of the form

$$\delta X(s) = \sin((M+N)\pi s)^2, \tag{5.26}$$

and

$$\delta\rho(s) = \frac{(M+N)\sin(2(M+N)\pi s)}{2\sqrt{N^2 + 2MN}}. \tag{5.27}$$

Here $\delta X(s)$ is the linearization of the X-component of the centerline, while $\delta\rho(s)$ is the linearization of the cylindrical polar coordinate $\rho^2 = Y^2 + Z^2$. Given that these formula are obtained from linearization about N-covered equilibria, the torus knot-type of the centerline of the linearized solution is determined. Our computations indicate that the torus knot-type of the full nonlinear solution is inherited from the linear problem (as could have been conjectured on general grounds).

5.3 Bifurcation Diagram and Configurations of the Ring

The formula (5.25) shows that on each trivial solution branch there is a countable infinity of simple bifurcation points. The main point of interest is to follow the branches of non-planar equilibria emanating from the known circular solutions. With the closed form formula of planar trivial solutions, we can start our computation anywhere on a trivial solution branch, and then numerically trace the bifurcating branches of non-planar equilibria. The result that was rather surprising to us was that the branch emanating from the Mth bifurcation on the N-covered ring with positive shear force and positive twist links to the Nth bifurcation point on the M-covered ring with positive shear force and negative twist, which we write symbolically as $(M, N, +) \leftrightarrow (N, M, -)$. There is an analogous branch linking representatives of the circle family with negative shear force. The behavior is further clarified in the illustrations.

Figure 5.2 (a) (Color figures are appended at the end of the article.) shows a bifurcation diagram including the non-planar $(1,1)$, $(1,2)$ and $(2,2)$ branches and parts of the planar branches representing single, and double covered circular configurations. The vertical and horizontal axes represent respectively the resultant shear force λ and the twisting moment m_3. The branches are colored by the writhe of the corresponding equilibrium. The curved branches correspond to non-planar equilibria, while the straight branches represent the trivial circular solutions. From equation (5.17) it can be seen that the straight lines of positive slope correspond to positive twist solutions, with the steeper line being the double covered case $N = 2$, while the lines with negative slope correspond to negative twist solutions satisfying (5.21). Figure 5.2(b) illustrates a bifurcation diagram, in the same projection but with a smaller scale, in which all solution branches with $(M + N) \leq 7$ are included.

These bifurcation diagrams were obtained with the software package PCR [13] that was designed to visualize the solution sets of parameter-dependent two-point boundary value problems as computed by AUTO or other programs. Solution branches are plotted in three dimensions, and Figures 5.2 (a) and (b) are actually planar projections of three dimensional figures in which the axis pointing outward represents the total energy E of the elastic rod. The three dimensionality of the bifurcation diagram is illustrated in Figure 5.2(c) which, as indicated by the red axes vectors, is a skew projection of the small solution set. In the bifurcation diagram with force, twist and energy as axes, the branches corresponding to the non-planar solutions are actually double covered, i.e., each point on a nontrivial solution branch actually represents two different configurations. Figure 5.2(c) illustrates this fact by plotting a perturbation (actually a small rotation in a four dimensional space) from having force, twist and energy along the three axes, so that the originally double covered, nontrivial solution branches are each split into two distinct branches. Figure 5.2 (d) depicts the physical configuration of the solution corresponding to the point on the $(2,5)$ branch in the bifurcation diagram of Figure 5.2 (b) that is indicated by the filled circle. The green curve represents the center line $\mathbf{r}(s)$, and the ribbon shows how the rod is twisting.

Our computations reveal that self-contact of the uniformly isotropic rod only arises in rather special, well-defined circumstances. The first possibility is that the entire rod is multiply covered, either on the planar circular solutions, or along an entire branch of non-planar equilibria. For example the topmost curved branch in Figure 5.2 (a) is the $(2,2,\pm)$ branch, which represents equilibria that are all double-covered scaled copies of single-covered solutions appearing on the $(1, 1, \pm)$ branch. The numerics indicate that multiple covering arises whenever the integers (M, N) are not relatively prime.

The second, and only other, possibility for self-intersection is at a single point on each non-planar branch, where an $(M + N)$-foil arises, i.e. a symmetric configuration with $M + N$ congruent lobes. In fact the centerline of all non-planar solutions is wound on a torus (or doughnut) of revolution embedded in three-space with the axis of symmetry being the force $\mathbf{n}$. The cross-section of the torus deforms as the loading parameter θ is varied. The integers (M, N) determine the torus knot type of the centerline in concordance with the knot type of the eigensolution at the bifurcation points on the branches of planar equilibria. The $(M + N)$-foil arises at one critical parameter value when the hole in the center of the torus pinches off (cf. Figures 5.6 and 5.10). The writhe is not defined at $(M + N)$-foils and has a point of discontinuity as the branch is traversed (cf. the coloring in Figure 5.2). The torus knot type switches at $(M + N)$-foils, and it is also close to this point that the numerics can be switched to a code that includes a model to preclude self-intersection as is described in Part II of this article. This behavior was known in the case $(M + N) = 2$, where the 2-foil is the figure eight, but for $(M + N) > 3$ we believe the conclusion to be original, with the case $(M + N) = 3$ being partially understood previously [33].

The full benefits of visualizing bifurcation sets with a software utility such as PCR can only be appreciated with the interactive capabilities of a graphics workstation, but we have included a selection of illustrations that depict some representative output of PCR. More examples can be found at the Web site `http://jacobi.umd.edu/pcr.html`. Figures 5.3–5.10 all illustrate certain features of the solution set to the loop boundary value problem. The five Figures 5.3, 5.5, 5.6, 5.7 and 5.8 each comprise four viewpoints of a single equilibrium. The four views comprise two elevations, a plan view and a skew-view (the axes reveal the relative orientations of each viewpoint). Each of the five figures illustrate an equilibrium for a different amount of imposed twist. Figure 5.4 shows a sequence of different configurations on the $(1, 1, \pm)$ branch from a single skew perspective as the load parameter θ is varied.

For isotropic rods the twist moment m_3 is constant. As previously mentioned in Section 3.3, whenever the value of the force $\mathbf{n}$ is prescribed, it is simple to verify that the configuration of the centerline $\mathbf{r}(s)$ depends upon the value of m_3, but is independent of the bending stiffness $K_3(s)$, and unstressed twist $\hat{u}_3(s)$. The values of K_3 and $\hat{u}_3$ do affect the twist rate $u_3(s)$ of the rod, as determined by equation (3.44) for the prescribed value of m_3. Figure 5.9 illustrates this phenomenon in the particular case of a uniform, isotropic rod. The three configurations shown arise for three different pairs of twisting stiffnesses and unstressed twist rates $(K_3, \hat{u}_3)$. The pairs of values are chosen so that the ribbon closes upon itself, i.e., the angle between $\mathbf{d}_1(0)$ and $\mathbf{d}_1(1)$ is a multiple of 2π. However the different configurations have different self-linking numbers.

Finally Figure 5.10 provides views of three configurations of a loop with high (M, N) values. We took $M = 12$ and $N = 13$ and imposed different twist loadings to obtain a 25–foil, and configurations on either side of the self-intersection.

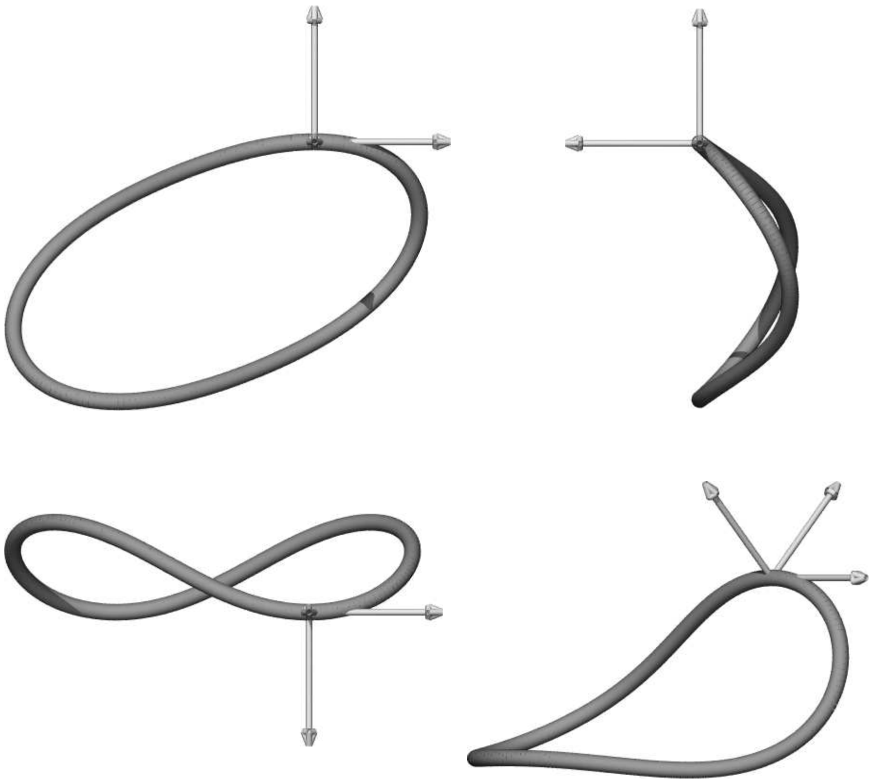

FIG. 5.3 *Four views of a typical configuration on the solution branch emanating from the* $(1, 1, +)$ *bifurcation point. It has left-right symmetry in both side elevations, and period two symmetry in the plan view. The symmetry classes of equilibria are fully described by Domokos [14].*

FIG. 5.4 *Different configurations all lying on the branch that links the* $(1,1,-)$ *and* $(1,1,+)$ *bifurcation points. The circle in the upper left is a negative twist solution, and the upper right solution is analogous to Figure 5.3. In the middle left there is a self-intersecting planar figure-eight solution, with another solution analogous to Figure 5.3 in the middle right, and finally the planar positive twist solution. The twist is monotone increasing from a negative to positive value through this sequence. In these calculations effects of self-intersection are ignored.*

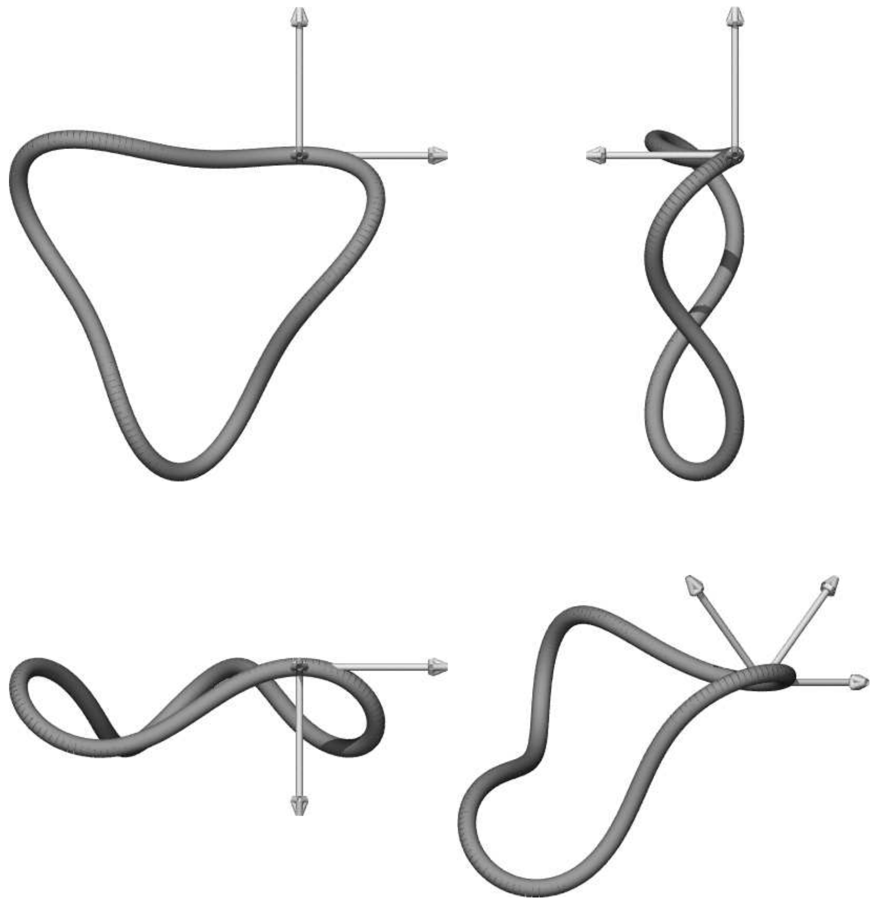

FIG. 5.5 *Figures 5.5, 5.6, and 5.7 show a sequence of three configurations on the branch linking the $(1,2,-)$ bifurcation point to the $(2,1,+)$ bifurcation point. Each figure depicts four views of the same equilibrium. All three configurations have period three symmetry in the plan view. The analogue of the self-intersecting figure-eight configuration is the self-intersecting trefoil shown in Figure 5.6. For twists slightly greater than the trefoil, the configuration becomes the non-intersecting trefoil knot shown in Figure 5.7, while the configuration shown in Figure 5.5 is unknotted.*

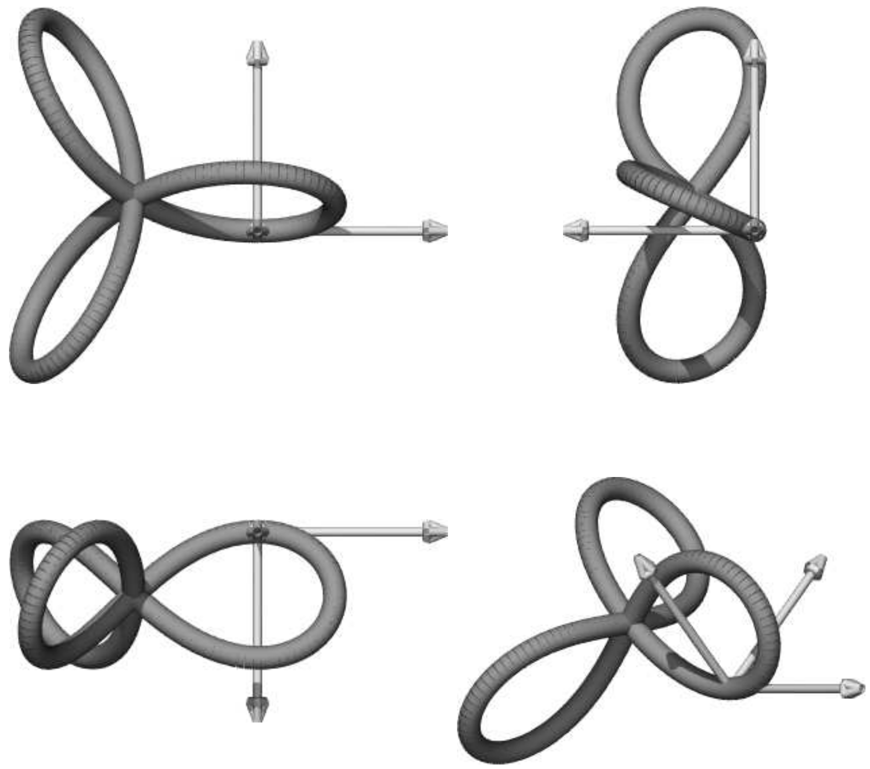

FIG. 5.6 *Figures 5.5, 5.6, and 5.7 show a sequence of three configurations on the branch linking the* $(1, 2, -)$ *bifurcation point to the* $(2, 1, +)$ *bifurcation point. Each figure depicts four views of the same equilibrium. All three configurations have period three symmetry in the plan view. The analogue of the self-intersecting figure-eight configuration is the self-intersecting trefoil shown here. For twists slightly greater than the trefoil, the configuration becomes the non-intersecting trefoil knot shown in Figure 5.7, while the configuration shown in Figure 5.5 is unknotted.*

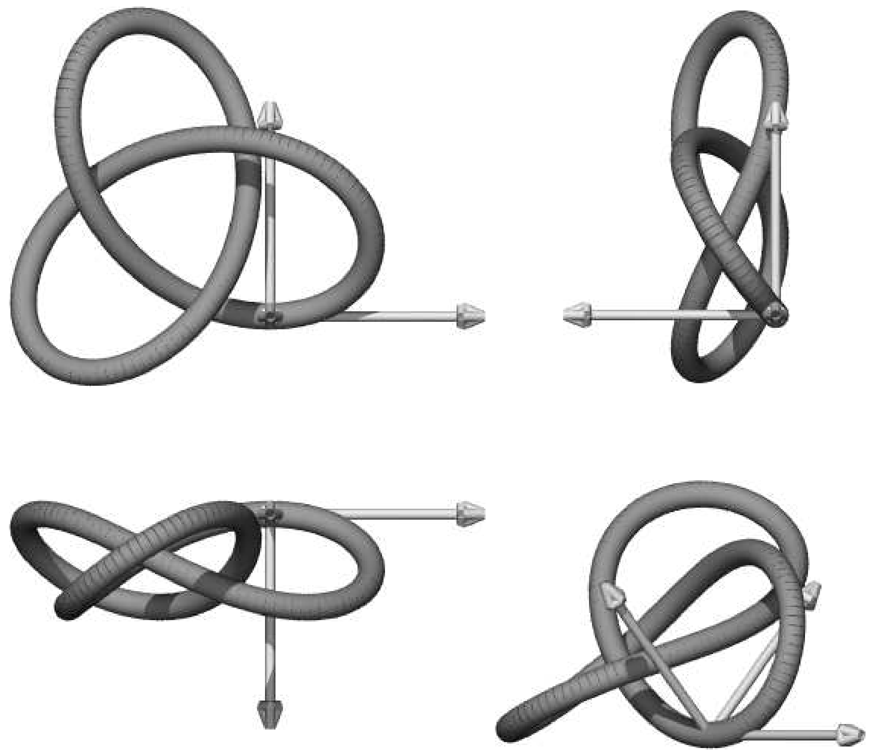

FIG. 5.7 *Figures 5.5, 5.6, and 5.7 show a sequence of three configurations on the branch linking the* $(1, 2, -)$ *bifurcation point to the* $(2, 1, +)$ *bifurcation point. Each figure depicts four views of the same equilibrium. All three configurations have period three symmetry in the plan view. The analogue of the self-intersecting figure-eight configuration is the self-intersecting trefoil shown in Figure 5.6. For twists slightly greater than the trefoil, the configuration becomes the non-intersecting trefoil knot shown in Figure 5.7, while the configuration shown in Figure 5.5 is unknotted.*

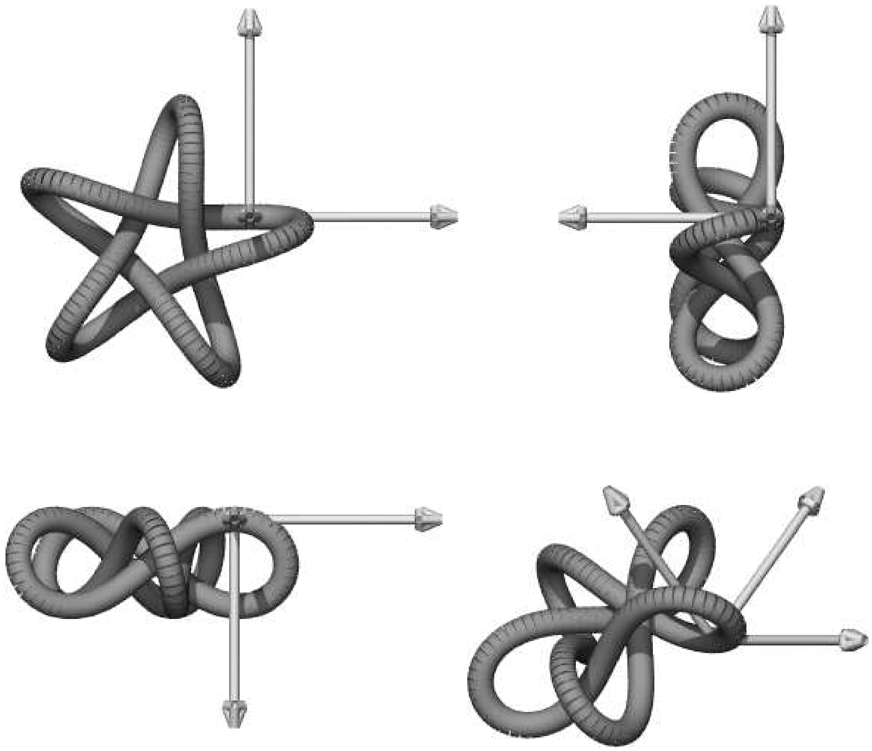

FIG. 5.8 *A knotted configuration on the* $(2,3,+)$ *to* $(3,2,-)$ *branch with five fold symmetry.*

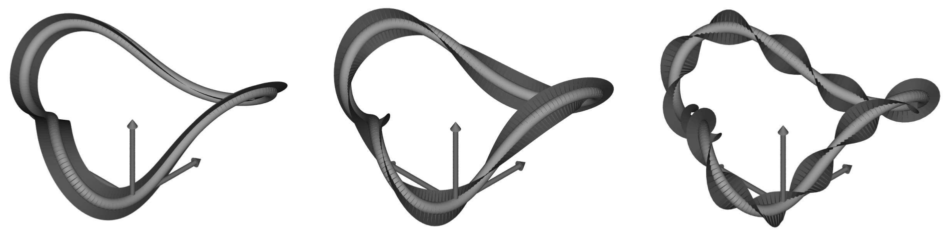

FIG. 5.9 *Three closed configurations of uniform, isotropic rods with different values of stiffness coefficient* K_3 *and unstressed twist rate* $\hat{u}_3$*. The centerlines* $\mathbf{r}(s)$ *are identical, but, as illustrated by the ribbon, the director frames have different twist rates* u_3*, and the solutions have different linking numbers.*

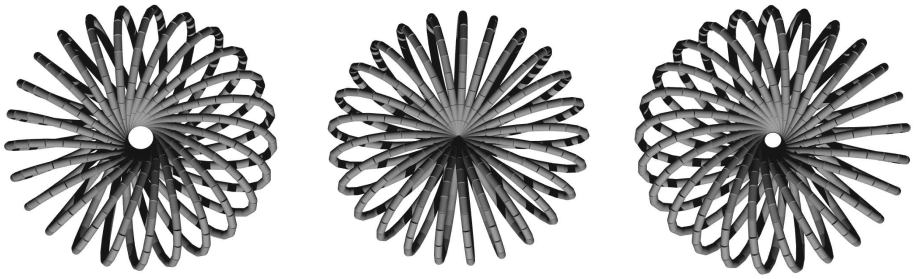

FIG. 5.10 *Configurations on the branch linking the* (12, 13, −) *and* (13, 12, +) *bifurcation points. The first configuration is before self-intersection occurs, the second is at self-intersection, and the third is after self-intersection and the knot type has switched.*

6 Symmetry Breaking in the Loop BVP

Our final computations concern symmetry breaking in the loop problem. The objective is to compute branches of equilibria when the rod is neither uniform, nor isotropic. This is the procedure that is applied in [28] to model effects of sequence dependent, unstressed shapes on the cyclization rates of DNA mini-circles. There is no difficulty with the appropriate boundary conditions; they are (5.1)—(5.4). The issue is to obtain starting points on each connected component of the perturbed solution set. The procedure we follow is the exact analogue of the symmetry breaking procedure for the strut BVP that was described in more detail in Section 4.6. We first introduce a homotopy parameter γ in the coefficients; here we considered the artificial example

$$K_1(s) = 0.1, \qquad K_2(s) = 0.1 + \gamma\, 0.2\,(0.75 - s)s. \tag{6.1}$$

We then run AUTO on equations (3.40) subject to boundary conditions (5.1)—(5.4), with the angle parameter θ fixed, continuation in the homotopy parameter γ, and starting from the planar trivial solution corresponding to the prescribed value of θ with $\gamma = 0$. For $\gamma = 0$ this problem is known to have a one-parameter family of non-isolated solutions generated by the symmetry of isotropy. (Recall that the trivial equilibria are fixed points of the translational symmetry so only a one–parameter isolation is present.) AUTO robustly traverses this one dimensional family, reporting bifurcation points at configurations where it is possible for γ to assume nonzero values. At these points, branches can be switched, and the homotopy parameter γ increased to one. Then γ can be frozen, and the angle θ activated as continuation parameter, to trace out branches of locally isolated solutions of (3.40) subject to boundary conditions (5.1)—(5.4).

The resulting bifurcation diagram is depicted in Figure 6.1, where we show the original isolated branches of the perfect problem in thin dark lines, and each connected component of the perturbed problem in a different color. The three coordinate axes represent the norm of the resultant force $|\mathbf{n}|$, the twisting moment $m_3(0)$, and the value of the Hamiltonian at $s = 0$. The symmetry related orbits, and the paths along which the homotopy parameter were varied are omitted (they are all extremely short on the scale of the Figure). Our conclusions are similar to the symmetry breaking for the strut BVP. However the symmetry orbit from each trivial solution now contains only two bifurcation points. This is the generic case that could have been anticipated; a circle of symmetry related critical points splits into a maximum and minimum on the circle. Moreover splitting from any trivial solution lying between two given bifurcation points leads to solutions on the same two branches of perturbed equilibria. In contrast, as $\gamma \to 0$ different connected components approach different segments of the trivial branches as partitioned by the perfect bifurcation points. Close to the bifurcation points the imperfect branches switch to shadowing the branches of non-planar equilibria of the perfect problem, before rejoining another planar segment. We found that the exact nature of the decoupling of the imperfect problem depended upon the exact perturbation chosen. However in all of the examples we computed, all of the perturbed branches were found to be of bounded extent and closed.

Of course our computations do not prove that all of the nearby connected components of the solution set of the perturbed problem were located, but it seems to be a plausible conjecture. In particular we did verify that no further components of imperfect solutions were generated by perturbing from a non-planar solution of the uniformly isotropic problem. That calculation is more intricate because if we attempt to switch immediately to the completely unsymmetric boundary conditions (5.1)–(5.4) from the completely symmetric boundary conditions (5.7)–(5.10), the starting point solution is embedded in a two parameter family of symmetry related solutions, and the one parameter numerical continuation routines implemented in AUTO failed immediately. The resolution is to break the two symmetries in two separate stages, and to have two homotopy parameters in the coefficient functions. It is most convenient to break uniformity first, and to insert an intermediate state of an isotropic, non-uniform rod. For example, instead of the family of coefficients (6.1), the two parameter family

$$K_1(s) = 0.1 + (\gamma_1 - \gamma_2)0.2(0.75 - s)s, \qquad K_2(s) = 0.1 + \gamma_1 0.2(0.75 - s)s. \tag{6.2}$$

can be taken. For $\gamma_2 = 0$ and $\gamma_1 \neq 0$, we obtain an isotropic, non-uniform rod, and for $\gamma_2 \neq 0$ we obtain a non-isotropic, non-uniform rod.

For this sequential splitting to work we must introduce boundary conditions that yield locally isolated solutions for isotropic, non-uniform rods. For such rods (3.45) is no longer an integral, but $m_3(s)$ still is. It can then be shown that the two conditions $\mathbf{d}_3(0) = \mathbf{d}_3(1)$ are implied by the single equation:

$$(\mathbf{m}(0) \times \mathbf{d}_3(0)) \cdot \mathbf{d}_3(1) = 0.$$

After writing this last expression in terms of the phase variables, it can further be shown that a set of fourteen boundary conditions that guarantee local isolation of solutions for isotropic, non–uniform rods, is:

$$\begin{cases} \mathbf{r}(0) = \mathbf{r}(1) = (0,0,0), \qquad (q_1(0), q_2(0), q_3(0)) = (0,0,0), \\ q_3(1) = -\sin(\theta/2), \qquad q_4(1) = -\cos(\theta/2), \\ \mu_1(0)[q_2(1)q_3(1) - q_1(1)q_4(1)] - \mu_2(0)[q_1(1)q_3(1) + q_2(1)q_4(1)] = 0, \\ n_2(0) = 0, \qquad \mu_4(0) = 0. \end{cases} \tag{6.3}$$

Under continuation in γ_1 with θ and γ_2 held fixed, and subject to boundary conditions (6.3), a circle of isotropy related solutions are found, and two bifurcation points are reported. At the bifurcation points, branches can be switched and γ_1 increased to 1, say. Then the problem is changed to boundary conditions (5.1)—(5.4), with γ_2 as continuation parameter. Each of the two starting points produces a circle of translation related equilibria with $\gamma_2 \equiv 0$, and on each circle there are two bifurcation points. Consequently we arrive at a total of four solutions of the completely non-symmetric problem. As it happens, each of these solutions lies on (a different) one of the four components that were obtained by splitting from the trivial branch, so no new equilibria were found by this procedure. The fact that the non-planar symmetric equilibria split to four solutions of the non-symmetric problem is consistent with topological arguments. The non-planar symmetric equilibria are representatives of a 2-torus of symmetry related critical points; generically such families split into four critical points when the symmetry is broken.

Using similar techniques it is also possible to consider uniform, but non–isotropic rods, for example the case when $K_1 \neq K_2$, and rods with intrinsic unstressed curvature in which $\hat{u}_1$ or $\hat{u}_2$ is non-zero. It should be stressed that while Figure 6.1 depicts solution branches of an imperfect problem in which the perturbations are comparatively small, once symmetry has broken our numerical methods are not restricted to small perturbations. As a sample of such cases Figure 6.2 illustrates configurations of three different rods that are respectively isotropic but non–uniform, uniform but non–isotropic, and non–uniform and non–isotropic. These computations involve large perturbations. In the first case the bending stiffnesses are non-constant $K_1(s) = K_2(s) = 0.1 + 0.6\,(s - 0.75)\,s$. The configuration is still a planar figure eight, but the two lobes are of different sizes. The second case has $K_1(s) \equiv K_2(s) \equiv 0.1$, $\hat{u}_1 = 0.21\pi$ and $\hat{u}_2 = 0.42\pi$, i.e., a constant intrinsic curvature. The configuration is a non–planar self–intersecting 'figure eight' with two lobes of equal size. Finally, the third case is neither isotropic nor uniform with bending stiffnesses $K_1(s) = K_2(s) = 0.1 + 0.35\,(s - 0.75)\,s$, and $\hat{u}_1 = 0.21\pi$ and $\hat{u}_1 = 0.42\pi$. The configuration is non–planar, with no self–intersection, and no symmetry.

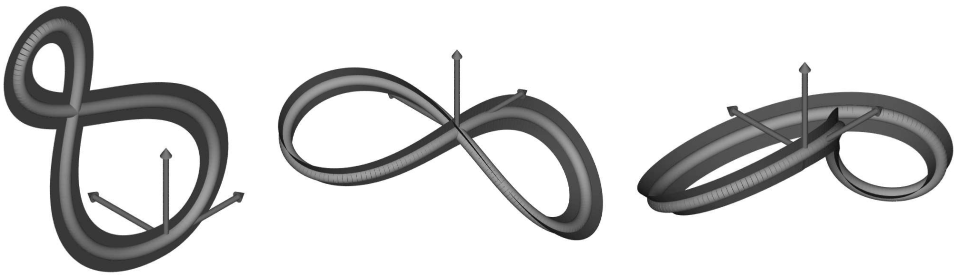

FIG. 6.2 *Configurations of three rods that are (from left to right) isotropic but non–uniform, uniform but non–isotropic, and non–uniform and non–isotropic. The configurations were all computed as perturbations of the planar figure-eight solution of a completely symmetric rod.*

7 Conclusions and Discussion

The purpose of this article has been to describe techniques for the computation of the equilibria of twisted elastic rods, with a particular emphasis on the case of a closed, twisted loop. The motivation for understanding this problem arises in the modelling of DNA, but we defer to other works, in particular [28] and other ongoing research, for analysis of the rather interesting questions of how accurately continuum elastic rod models actually mimic DNA behavior. The eventual application to DNA did, however, motivate the generality of the formulation we developed, which encompasses natural curvature and twist, and non-uniformity (as might arise from sequence dependence), anisotropic bending stiffnesses, and nonlinear constitutive relations. In particular, we do not use the celebrated formula $Lk = Tw + Wr$ (see for example the review article [32] and references therein), which, when used in elasticity computations, restricts attention to the case of isotropic, uniform rods for which the twist rate u_3 of solutions is constant. While we here assume an unshearable, inextensible rod, our model does extend straightforwardly to the shearable, extensible case [7]. Self-contact is a crucial feature of many DNA configurations, and models of such phenomena provide the motivation for the extensions precluding self-intersection that are presented in Part II of this work [24].

The primary mathematical and computational novelty of our analysis centers on the interplay between continuous symmetries, the Hamiltonian formulation of the two-point boundary value problem (BVP), and the use of efficient numerical continuation techniques. We here work entirely within the particular context of the equations governing the elastic rod, and we make no precise statement about more general problems, but it seems clear that the ideas underlying our approach carry over to the context of nonlinear, parameter-dependent, two-point BVP for ordinary differential equations of Hamiltonian form. The presence of a high degree of continuous symmetry is related to the presence of explicitly known solutions of the BVP, which can serve as starting points for numerical continuation. The presence of continuous symmetry also yields a large connected solution set, which is again suitable for continuation techniques. On the other hand the same continuous symmetries that provide the starting point and connectedness that are so compatible with numerical continuation, also imply that all solutions are non-isolated at a given continuation parameter. This non-isolation raises serious difficulties for standard numerical packages, and necessitates some care in the numerical continuation approach.

The difficulty of non-isolation is resolved by exploiting a combination of the Hamiltonian formulation of the equations and the very same symmetries that gave rise to the difficulties in the first place. For Hamiltonian systems, or any other equivalent formulation, (variational) symmetries generate integrals of the ordinary differential equations. We use these integrals to develop appropriate modifications of the boundary conditions in order to allow effective numerical continuation in the presence of continuous symmetries.

Our exploitation of the Euler parameter (or quaternion) parameterization of the proper rotation group $SO(3)$ plays an important role in our computations. The Euler parameters provide a four dimensional description of the three dimensional group. Consequently the appropriate Lagrangian is not strictly convex in the variables that play the role of generalized velocities. Accordingly the transformation to the Hamiltonian form requires some care. By addressing this difficulty in the analysis, we arrive at a formulation that is particularly amenable to numerics. The actual numerics are then performed by applying the standard method of collocation as implemented in the continuation package AUTO [10]. Our experience with this code was exceptionally good, particularly in the calculation of symmetry–breaking, where difficulties with numerical ill-conditioning might have been anticipated. We attribute this good behavior to a felicitous combination of three features, namely (i) the first order equations are in the form of a Hamiltonian system (with respect to evolution in arc-length), (ii) the collocation method is equivalent to a Gaussian Runge-Kutta algorithm [38] which is both symplectic and exactly conserves quadratic integrals [31], and (iii) due to our use of Euler parameters to parameterize rotation matrices, and with the single exception of (3.45), all of the several integrals of the problem are quadratic functions of the phase variables. The exact numerical invariance of these quadratic integrals apparently gives rise to good stability and error control. (Of course in practice the collocation equations are only solved to some prescribed tolerance, but it this then this tolerance, and not the discretization error, that controls the error in the quadratic invariants.) The numerical invariance of quadratic integrals at the mesh points can also be used as one basis for an effective mesh refinement strategy. However these features only become crucial in our computations of self-contact that are described in Part II of this work.

Most of our computational efforts have been directed to computing the quite complicated solution set arising for the completely integrable case of a uniformly isotropic loop. Indeed for our approach using parameter continuation, this case is in some ways the hardest one to compute. The analytic form of the circular solution for the uniformly isotropic rod is well-known, but we believe our computation of the higher non-planar modes of the solution set, and of the general pattern of connectivity of the non-planar branches to be original. Our numerical computations demonstrate that each non-planar branch is of finite extent and terminates at both end points in a configuration that is a planar circular solution, often multiply covered, according to the rule $(M, N, +) \leftrightarrow (N, M, -)$, i.e. the branch emanating from the Mth bifurcation point on the N-covered circle with positive twist connects to the

Nth bifurcation point on the M-covered circle with negative twist. When M and N have a common divisor the entire non–planar branch involves multiply covered solutions. The only non-circular, non-multi-covered configurations at which the rod self-intersects are precisely one configuration on each non-planar solution branch. At this self-intersecting solution the centerline of the configuration forms an $(M+N)$-foil, i.e. a symmetric figure with $(M+N)$ congruent lobes that all intersect at a single central point (cf. Figure 5.6 for the case of a 3– or trefoil). The configurations on each segment of a branch of singly covered, non–planar solutions have an associated torus knot type that is inherited from the associated, and explicitly known, eigenfunction at the bifurcation point at each end of the branch. In the interior of each branch, the torus knot type changes only at the self-intersecting $(M+N)$-foil configuration.

The higher modes in this bifurcation diagram are of some interest because experiments with highly flexible wires indicate that when effects of self-contact are included, some of the $(M+N)$-foil solutions are stable at least for $(M+N) \leq 14$. The classification of which equilibria are stable, both in the presence and absence of self-contact, is an interesting, largely open question, in which investigations are ongoing.

The Hamiltonian formulation of the equations governing rod equilibria that we have presented encompasses the possibility of a general class of nonlinear hyper-elastic constitutive relations. However, for computation a particular choice of constitutive relation must be made, and we have chosen to restrict attention to the case of linear elasticity, while of course retaining the full geometric nonlinearity in the problem. In the statics of rods the equilibrium equations can be nondimensionalized with respect to both length and force scales. Accordingly in a linearly elastic, uniformly isotropic rod in which $K_1 = K_2$ are constant and $\hat{u}_1 = \hat{u}_2 = 0$, we may assume with no loss of generality that the undeformed arc-length is one, $0 \leq s \leq 1$, and that $K_1 = 1$. The only free parameters are then the nondimensionalized twist stiffness $K_3(s)$ (or equivalently the ratio $K_3(s)/K_1$), and the intrinsic twist rate $\hat{u}_3(s)$. However, as previously remarked, using the symmetry of isotropy it is straightforward to verify that as $\hat{u}_3(s)$ and $K_3(s)$ are varied the axis (or centerline) of any equilibrium is unchanged, and the directors merely rotate about the tangent vector at a different (and explicitly determined) rate. In this sense a computation of the solution set of the two-point BVP governing equilibria of a uniformly isotropic rod for any constant values of $\hat{u}_3$ and K_3, contains practically all the information for a solution with general $\hat{u}_3(s)$ and $K_3(s)$. For other constant values of $\hat{u}_3$ and K_3 the solution to the BVP can be found in closed form, and for s-dependent coefficients a single initial value problem must be solved.

The solution set for uniformly isotropic rods is of intrinsic interest, but, perhaps more importantly, it can also be exploited as an organizing center for computation of solutions in models where each of the symmetries is broken. In particular any solution for the integrable case can be used as a starting point for symmetry breaking via parameter continuation in the coefficients, with the consequence that equilibria in all the non-integrable cases can also be computed. That is the procedure followed in the detailed modelling of DNA presented in [28]. Furthermore, when the model is modified to preclude self-intersection of the rod, as in [24], the solution set for the uniformly isotropic rod can be used to generate equilibria of prescribed torus knot type, and prescribed linking number, for non-uniform rods with arbitrary unstressed configurations and stiffness coefficients.

Acknowledgments: It is a pleasure for the authors to be able to thank Gabor Domokos and the members of the Numerical Analysis Laboratory in the Institute for Physical Sciences and Technology, especially Donald Dichmann, Oscar Gonzalez, Rob Manning, Kathleen Rogers and Randy Paffenroth, for their valuable contributions to this article.

References

[1] S.S. Antman, *Nonlinear Problems of Elasticity*, (Springer–Verlag, 1994).

[2] U. Ascher, J. Christiansen & R.D. Russell, *Collocation software for boundary value ODE's*, *ACM TOMS 7*, No. 2, 209, (1981).

[3] W.R. Bauer, R.A. Lund & J.H. White, *Twist and Writhe of a DNA Loop Containing Intrinsic Bends*, *Proc. Natl. Acad. Sci. USA*, **90**, (1990), pp. 833-837.

[4] C.J. Benham, *Onset of writhing in circular elastic polymers*, *Phys. Rev. A*, **39**, (1989), pp. 2582-2586.

[5] W.J. Beyn & E.J. Doedel, *Stability and multiplicity of solutions to discretizations of nonlinear ordinary differential equations*, *SIAM J. Sci. Stat. Compt. 2*, No. 1, (1981), pp. 107–120.

[6] D.J. Dichmann, *Hamiltonian Dynamics of an Elastica and Stability of Solitary Waves*, *Ph. D. thesis, University of Maryland*, (1994).

[7] D.J. Dichmann, Y. Li, & J.H. Maddocks, *Hamiltonian formulations and symmetries in rod mechanics*, in *Mathematical Approaches to Biomolecular Structure and Dynamics*, *The IMA Volumes in Mathematics and Its Applications*, **82** (1996) Eds. J.P. Mesirov, K. Schulten, & D.W. Sumners. pp. 71–113

[8] D.J Dichmann, J.H. Maddocks & R.L. Pego, *Hamiltonian Dynamics of an Elastica and the Stability of Solitary Waves*, *Arch. Rational Mech. Anal.* To appear.

[9] P.A.M. Dirac, *On generalized Hamiltonian dynamics*, *Can. J. Math.*, **2**, (1950), pp. 129-148.

[10] E. Doedel, *AUTO 86 User Manual*, *Caltech, Dept. Applied Mathematics*, (1986).

[11] E.J. Doedel, H.B. Keller & J.P. Kernevez, *Numerical analysis and control of bifurcation problems (I) Bifurcation in finite dimensions*, *International Journal of Bifurcation and Chaos*, Vol. 1, No. 3, (1991), pp. 493–520.

[12] E.J. Doedel, H.B. Keller & J.P. Kernevez, *Numerical analysis and control of bifurcation problems (II) Bifurcation in infinite dimensions*, *International Journal of Bifurcation and Chaos*, Vol. 1, No. 4, (1991), pp. 745–772.

[13] G. Domokos & R. Paffenroth, Case study: Visualization for Boundary Value Problems in *IEEE Visualization '94 Conference Proceedings*, Ed. R. D. Bergeron and A. E. Kaufman (IEEE Computer Society Press, 1994) pp. 345–348

[14] G. Domokos, *A group–theoretic approach to the geometry of elastic rings*, *J. Nonlinear Science*, to appear.

[15] J. Douglas Jr. & T. Dupont, *Collocation methods for parabolic equations in a single space variable*, *Lecture Notes in Mathematics*, 385, (Springer–Verlag, 1974).

[16] H. Goldstein, *Classical Mechanics*, Second Edition, (Addison–Wesley, 1981).

[17] A.A. Ilyukhin, *Spatial problems of non-linear theory of elastic rods*, (Kiev, Naukova Dumka, 1979). [in Russian]

[18] R. D. James, *The equilibrium and post–buckling behavior of an elastic curve governed by a non–convex energy*, *J. Elasticity 11*, (1981), pp. 239–269.

[19] F. Jülicher, *Supercoiling transitions of closed DNA*, *Phys. Rev. E*, **49**, (1994), pp. 2429-2435.

[20] T. R. Kane, P. W. Likins & D. A. Levinson, *Spacecraft Dynamics*, (McGraw–Hill, 1983).

[21] L.D. Landau & E.M. Lifshitz, *Theory of Elasticity*, (Pergamon Press, 1970).

[22] J. Langer & D. Singer, *Lagrangian Aspects of the Kirchhoff Elastic Rod*, *SIAM Review*, to appear.

[23] M. LeBret, *Catastrophic Variation of Twist and Writhing of Circular DNAs with Constraint?*, *Biopolymers*, **18**, (1979,) pp. 1709-1725.

[24] Li, Y. & J.H. Maddocks. On the Computation of Equilibria of Elastic Rods, part II: Effects of self-contact. In preparation.

[25] A.E.H. Love, *A Treatise on the Mathematical Theory of Elasticity*, (Dover, 1944).

[26] J.H. Maddocks, *Stability of nonlinearly elastic rods*, *Arch. Rational Mech. Anal.*, 85(4), (1984), pp. 180–198.

[27] J.H. Maddocks & D.J. Dichmann, *Conservation Laws in the Dynamics of Rods*, *Journal of Elasticity*, **34**, (1994), pp. 83-96.

[28] R.S. Manning, J.H. Maddocks, and J.D. Kahn, *A Continuum Rod Model of Sequence-Dependent DNA Structure*, *J. Chem. Phys.*, submitted.

[29] W.K. Olson, *Simulating DNA at low resolution*, *Current Opinions in Structural Biology* **6**, (1996), pp. 242–256.

[30] P.M. Prenter, *Splines and Variational Methods*, (John Wiley & Sons, 1975).

[31] J.M. Sanz-Serna & M.P. Calvo, *Numerical Hamiltonian Problems*, (Chapman & Hall, 1994).

[32] T. Schlick, *Modeling Superhelical DNA: Recent Analytical and Dynamical Approaches*, *Current Opinions in Structural Biology*, **5**, (1995) pp. 245–262.

[33] T. Schlick, W.K. Olson, T. Westcott & J.P. Greenberg, *On Higher Buckling Transitions in Supercoiled DNA*, *Biopolymers*, 34, (1994), pp. 565-597.

[34] Y. Shi, & J.E. Hearst, *The Kirchhoff elastic rod, the nonlinear Schrödinger equation, and DNA supercoiling*, *J. Chem. Phys.*, **101**, (1994), pp. 5186-5200.

[35] E.L. Starotsin, *Three-Dimensional Conformations of Looped DNA in an Elastomechanical Approximation*, *Proc. 2nd International Conference on Nonlinear Mechanics*, Edited by Chien Wei-zang, (Peking University Press, 1993).

[36] H. Tsuru, *Equilibrium Shapes and Vibrations of Thin Elastic Rods*, *J. Phys. Soc. Japan*, **56**, (1987), pp. 2309-2324.

[37] M. Wadati, & H. Tsuru, *Elastic Model of Looped DNA*, *Physica D*, **21**, (1986), pp. 213-226.

[38] R. Weiss, *The application of implicit Runge–Kutta and collocation methods to boundary problems*, *Math. Comp.*, **28**, (1974), pp. 449–464.

[39] Y. Yang, I. Tobias & W.K. Olson, *Finite Element Analysis of DNA Supercoiling*, *J. Chem. Phys.*, **98**, (1993), pp. 1673-1686.

[40] E. E. Zajac, *Stability of Two Planar Loop Elasticas*, *Trans. ASME, J. Appl. Mech*, **E** 29, (1962), pp. 136–142.

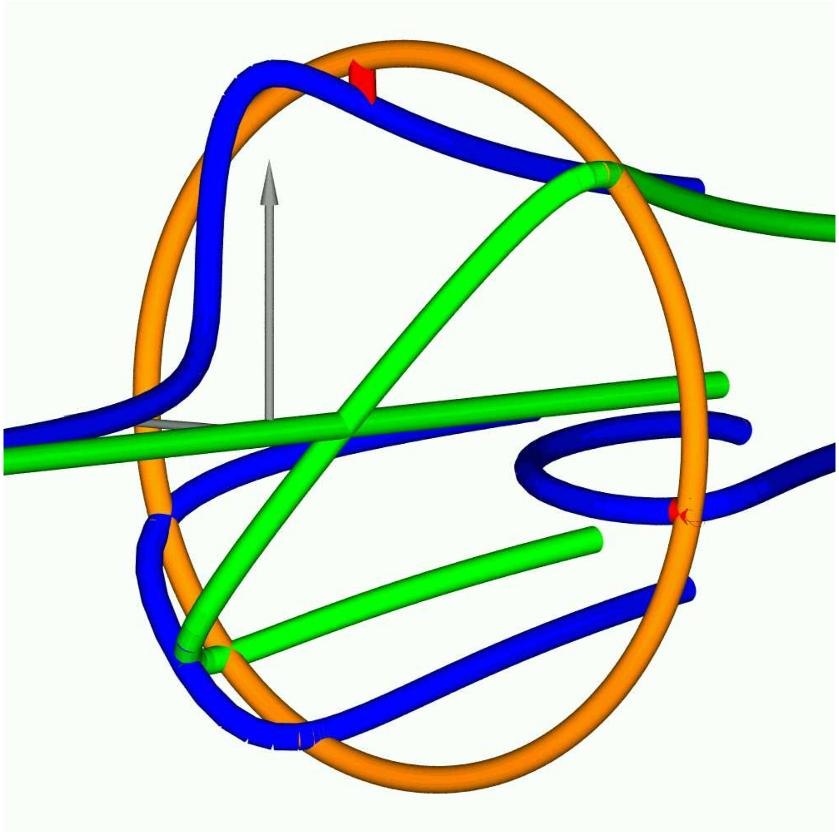

FIG. 4.4 *Solution branches of both the isotropic and non–isotropic strut boundary value problems. The solution curves are projected to the three-dimensional space* $(x(1), y(1), \lambda)$. *Equilibria of the symmetric strut are colored green; both the trivial branch and the representatives of the nontrivial solutions selected by the boundary condition (4.6) are shown. The circular orange segment corresponds to further solutions of the symmetric problem that are tracked by continuation in the imperfection parameter* γ *starting from an* $X + Y = 0$ *equilibrium. There are four bifurcation points on this circle, at which the computations can be switched to the* $\gamma \neq 0$ *branches that are shown in red (only two of the these rather short segments are actually visible in the chosen perspective). Finally, once the desired value* $\gamma = 1$ *of the imperfection parameter is reached, the blue branches representing components of the perturbed bifurcation set are computed by switching back to the load as continuation parameter, now with the original boundary conditions (4.1). The apparent intersection of the blue and green branches appearing in the bottom left is an artifice of the particular projection, and the finite radius of the tubes that have been drawn.*

CAPTION FOR FIGURE 5.2 *Parts a) and b) show the projection of the bifurcation set that arises when the force* $n_1(0)$ *(ordinate) is plotted against twist* m_3 *(abscissa). Figure a) is a detail of part b) close to the origin. The curves are colored according to their writhe. The straight lines correspond to planar 'trivial' circular solutions that are covered an integer* N *number of times, with either positive or negative twist. The other solution branches correspond to nonplanar configurations that arise at bifurcation points on the* N *covered trivial branch that can be indexed as* $(M, N, \pm)$*. The nonplanar branches link the bifurcation points on the trivial planar solutions according to the relation* $(M, N, +) \leftrightarrow (N, M, -)$*. All branches for* $(M + N) \leq 7$ *are shown in part b).*

The reconstructed physical configuration depicted in part d) corresponds to the point indicated by the filled circle in the top center of the bifurcation diagram shown in part b). The green tube represents the center line of the configuration, and the blue ribbon illustrates the twist of the director frame.

Part c) is a perspective view of a composite rotation of the plan view of the solution set shown in part a). First, there is a large rotation in $(m_3,\, n_3(0),\, E)$ *space (where* E *is the energy of the equilibrium). Second, a small four-dimensional rotation is applied as a perturbation to reveal that the branches of non-planar equilibria are in fact double covered in the projection used in parts a) and b).*

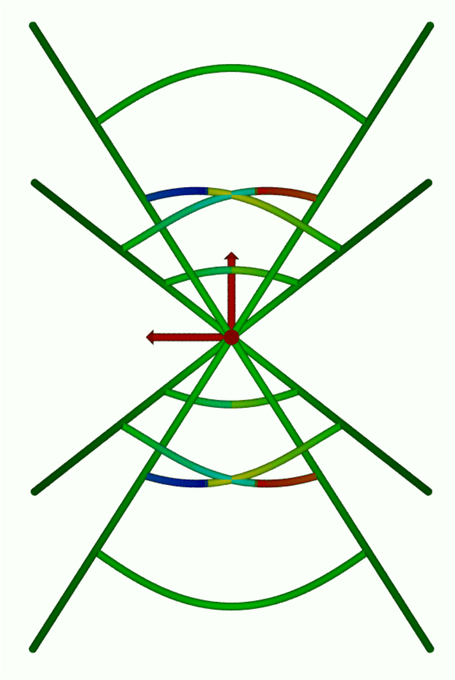

Figure 5.2 (a)

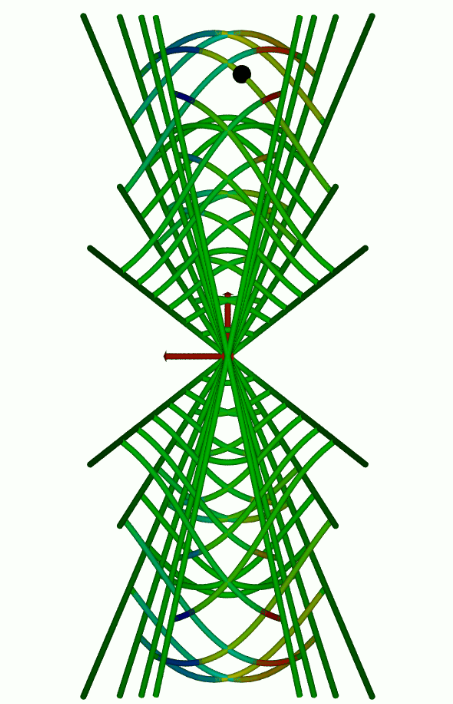

Figure 5.2 (b)

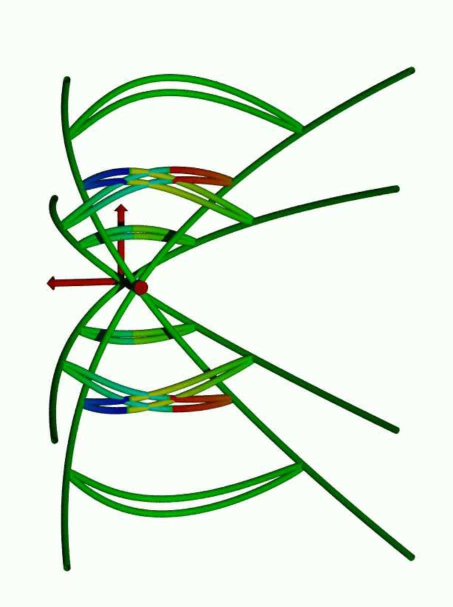

Figure 5.2 (c)

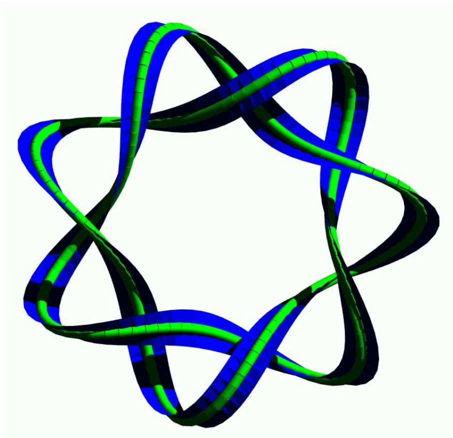

Figure 5.2 (d)

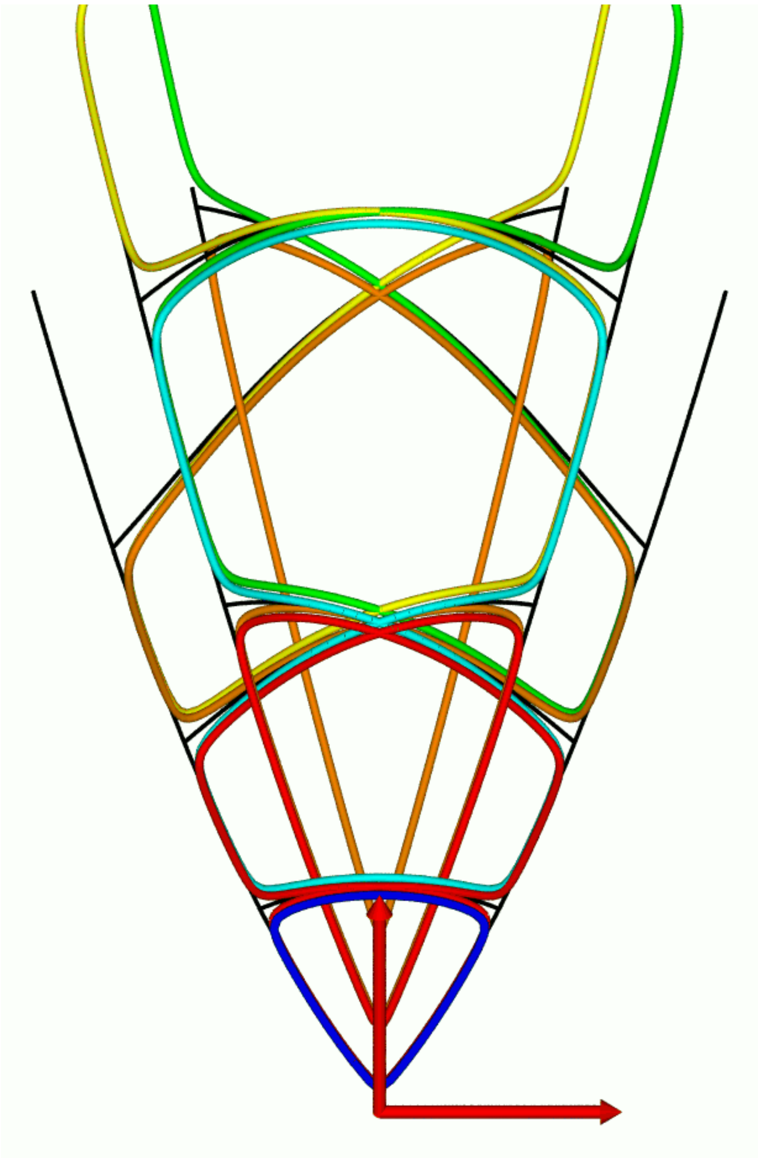

FIG. 6.1 *If the rod is not both uniform and isotropic, the highly connected, perfect bifurcation set illustrated in Figure 5.2 breaks into a solution set with a number of disconnected components. Here each component of the perturbed diagram is colored differently, while the original perfect diagram is shown in black. The solution curves are drawn in* $(|\mathbf{n}|, E, m_3(0))$ *space with* m_3 *horizontal, and the vertical being a composite of* $|\mathbf{n}|$ *and* E*.*